ELSEVIER

Journal of Fluids and Structures 26 (2010) 954–978

JOURNAL OF FLUIDS AND STRUCTURES

www.elsevier.com/locate/jfs

First- and second-order analysis of resonant waves between adjacent barges

L. Sun[1], R. Eatock Taylor*, P.H. Taylor

Department of Engineering Science, University of Oxford, Parks Road, Oxford OX1 3PJ, UK

Received 2 September 2009; accepted 29 May 2010
Available online 7 July 2010

Abstract

Water wave diffraction by two parallel closely spaced rectangular barges is investigated, to characterise the general problem of LNG offloading from a floating plant into a shuttle tanker. It is well known that large free-surface motions, in the gap between the hulls, are predicted by diffraction theory; in model tests amplitudes of at least five times that of the incident wave amplitude have been observed. A second-order diffraction calculation is used, based on a quadratic boundary element method, to examine the behaviour of this characteristic configuration and to examine the influence of spacing between the hulls. The free-surface near-resonant behaviour at first and second order is interpreted in the context of simple linear analytical solutions for three-dimensional flow in an open-ended gap.

Keywords: Barges; Wave-trapping; Second-order diffraction

1. Introduction

The aim of the work described here is to investigate hydrodynamic phenomena that can occur when vessels involved in the transfer of LNG are very closely spaced. A characteristic case might be a floating rectangular barge of length 400 m, parallel to a tanker of length 250 m and a gap between them of as little as 4 m. If one were to model the related very simple problem of two infinitely long cylinders with fluid between and below them, intersected by the free surface, one could immediately deduce that resonant standing waves (''trapping'') can exist across the gap. Furthermore, the actual geometry is such that three-dimensional effects can be important, and near-resonant standing waves can also exist along the length of the gap. Because the ends of the gap are open, energy can escape from between the hulls, and pure trapping cannot exist. But for a thin gap very little energy escapes, and potential flow theory predicts that very large amplitudes of free-surface motion within the gap can be set up by incident regular waves.

This phenomenon has of course long been recognised, although for the most part it has been the resonances across the gap that have attracted attention. The first numerical investigation of the three-dimensional (3-D) problem was probably that of Newman and Sclavounos (1988), and more recently the interactions between multiple closely spaced bodies have been further studied (e.g. Kashiwagi (2007)). Koo and Kim (2005) have shown the importance of modelling the fully coupled dynamics if reliable predictions are to be made of wave diffraction and radiation forces on each vessel,

*Corresponding author.
E-mail address: r.eatocktaylor@eng.ox.ac.uk (R. Eatock Taylor)..
[1]Now at National University of Singapore.

0889-9746/$ - see front matter © 2010 Elsevier Ltd. All rights reserved.
doi:10.1016/j.jfluidstructs.2010.06.001

and hence of the relative motions of closely spaced bodies. Such relative motions (both horizontal and vertical) affect both the specification of the moorings and the design of the LNG transfer systems. Nor is practical interest confined to forces and motions of the closely spaced vessels: prediction of the behaviour of the local free surface is also important. Teigen and Niedzwecki (2006) have calculated the wave elevations near closely spaced barges, including second-order sum-frequency components (general expressions for the second-order wave elevation are given, for example, by Sulisz and Hudspeth (1993) or Zhang and Williams (1996)). The results suggested the possibility of remarkably high amplifications of local wave elevation, with the potential for damage to equipment. Attempts have been made to account for the inevitable (and highly desirable!) damping in the real flow situation (associated with frictional drag and separation effects at corners) and limitations on resonant amplitudes imposed by nonlinear effects. A common approach is to use an artificial damping layer on the free surface in the gap (e.g. Lee and Newman (2005), Pauw et al. (2007)), though there would seem to be no satisfactory way of knowing *a priori* what amount of damping to incorporate. Experiments have been undertaken to address this, both for the two-dimensional situation (Kristiansen and Faltinsen, 2007) and for the near-resonant behaviour in the 3-D problem (e.g. Pauw et al. (2007)). The latter highlights the difficulty of characterising the damping layer. Indeed in some situations, as found by Kashiwagi et al. (2005) and Hong et al. (2005), good comparisons between experiments and potential flow predictions can be obtained without recourse to any artificial damping layer. Kristiansen and Faltinsen (2008) have compared experimental data with results from a two-dimensional numerical analysis using vortex tracking to investigate the effects of damping due to the following mechanisms: energy transfer to higher modes associated with nonlinear effects in the free-surface conditions; the effects of the boundary layer on each hull; and damping due to flow separation, all in the context of piston-like sloshing in the gap. For the cases considered the results show that much of the most significant source of discrepancies between linear theory and measured free-surface responses is flow separation. This led to reduction of the resonant peaks of sloshing motion by about 40% at the largest forcing amplitude and about 30% for the lowest amplitude. It is striking that resonant magnifications of up to 10 times were observed in their experiments.

Here we attempt to shed further light on the phenomenon of possibly large near-resonant amplifications. A simple configuration of two rectangular boxes – basic barges – is used to characterise the fundamental sloshing behaviour between two vessels. Extensive results are computed using a frequency domain three-dimensional boundary element code DIFFRACT developed as a research tool over several years (Eatock Taylor and Chau, 1992; Eatock Taylor and Huang, 1996; Zang et al., 2006). The program is based on use of quadratic elements, and one or two planes of geometric symmetry may be exploited to reduce computational times. The problem of irregular frequencies, to which such frequency domain models may be prone, is overcome using a method similar to that of Sun et al. (2008a). First- and second-order loads and free-surface elevations may be computed. Verification of the program has been demonstrated, for example in the above-mentioned publications where results are compared with those from other theoretical and experimental models. In the present paper the numerical results are set in context by comparison with some theoretical results from two simple analytical models. It has been noted by others that the problem is closely related to that of the moonpool, which was comprehensively investigated by Molin (2001) using linear potential flow analysis. Attempts have previously been made to use the predictions of moonpool resonant frequencies to inform the understanding of the gap resonances. But the boundary condition at the ends of the gap differs from that for the moonpool. A more complex analysis has been developed by Saitoh et al. (2000), using an asymptotic matching technique, to represent the flow field near the ends of the gap. Other work related to this problem is that of Miao et al. (2001), Zhu et al. (2005, 2006), Wang and Wu (2008), Saitoh et al. (2006) and Lu et al. (2008). The moonpool analysis of Molin (2001) has been extended by Molin et al. (2002), and this is the basis for the first simple model with which we make comparisons. We also compare with the theory (Mei, 1983) of a long channel penetrating a breakwater.

2. Results for twin boxes

2.1. Configuration and properties

The configuration consists of two parallel rectangular boxes arranged as indicated in Fig. 1. The dimensions are characteristic of the overall dimensions of a large LNG carrier. Cases of different drafts were considered in order to assess the influence of that parameter on the hydrodynamics. Different spacings of the boxes (i.e. the widths of the rectangular gap between them) were used, from the closest (4 m) to a spacing of 18 m representing a potential situation during an approach. The water depth was 50 m. Cases of the boxes fully fixed and freely floating were investigated. The dynamic parameters governing the latter behaviour are given in Table 1. The additional roll damping shown in this table is intended to represent the effects of viscosity, estimated using an empirical model developed by Tromans (2008).

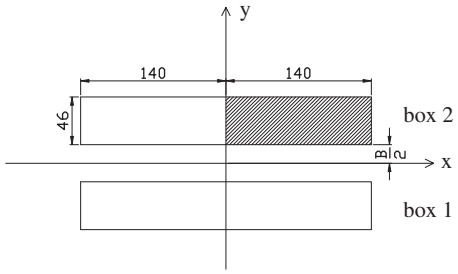

Fig. 1. General arrangement of two boxes.

Table 1
Properties of boxes.

Length (m)	280		
Breadth (m)	46		
Draft (m)	16.5	33.0	50.0
Vertical of centre of gravity (m)	16.5		
Transverse radius of gyration (K_{rr}) (m)	14.0		
Additional roll damping (N m/rad/s)	3.562×10^9		

2.2. Summary of numerical method

Based on a boundary element representation, the program DIFFRACT computes first- and second-order hydrodynamic quantities, including free-surface elevation on and around the diffracting structures. Quadratic boundary element meshes for the DIFFRACT linear analysis are required on the body surface and the inner free surface of a surface-piercing structure, as shown for a typical mesh in Fig. 2(a) and (b), respectively, for the twin box problem. Corresponding finer meshes are shown in Fig. 2(c) and (d). Only a quadrant representing one-half of one hull is modelled explicitly, because geometrical (but not hydrodynamic) two-plane symmetry is exploited here to represent the other three quadrants implicitly. It is then convenient to use an origin of coordinates at the centre of the gap, so that the x and y axes are in the planes of symmetry. The meshes in Fig. 2 illustrate appropriate refinement of the quadratic elements near the corners of the box and on the inner waterplane area adjacent to the gap. Some interior nodes within "discontinuous elements" may be noted adjacent to the waterline in Fig. 2(b) and (d): these are used in the procedure implemented in DIFFRACT to avoid the awkward problem of irregular frequencies (Subia et al., 1995; Sun et al., 2008a). Convergence has been carefully considered in obtaining the results below. This is illustrated in Fig. 3, where the frequency dependence of the free-surface elevation half-way along the gap is shown based on the two meshes in Fig. 2. Head sea and beam sea cases are given in Fig. 3(a) and (b), respectively, over the highest range of frequencies considered in this study. It may be seen that the coarser Mesh 1 yields results that differ very little from those computed with Mesh 2.

2.3. First-order wave forces

2.3.1. Comparisons with single box

We first show the major change to wave forces resulting from bringing the boxes into close proximity. Fig. 4 shows the dependence on frequency ω of the sway and heave force magnitudes, and the roll moment, acting on the two boxes in beam seas propagating in the positive y direction; the figure also shows equivalent results for a single box having the same properties. The forces are in Newtons divided by ρgA, and the moment is in N m divided by ρgA, where ρ is the density of water, g the acceleration due to gravity and A the incident wave amplitude. The draft is 16.5 m and the two boxes are at 18 m spacing. Box 1 is upwave of box 2. Hydrodynamic interactions between the two boxes lead to the maximum sway force on each box being more than double that on the isolated box. The roll moment is increased even more over a similar frequency range around $\omega = 0.52$ rad/s. Some sharp peaks in the sway force and roll moment plots may also be clearly seen above 1.3 rad/s. The behaviour in this latter range of frequencies will be discussed below.

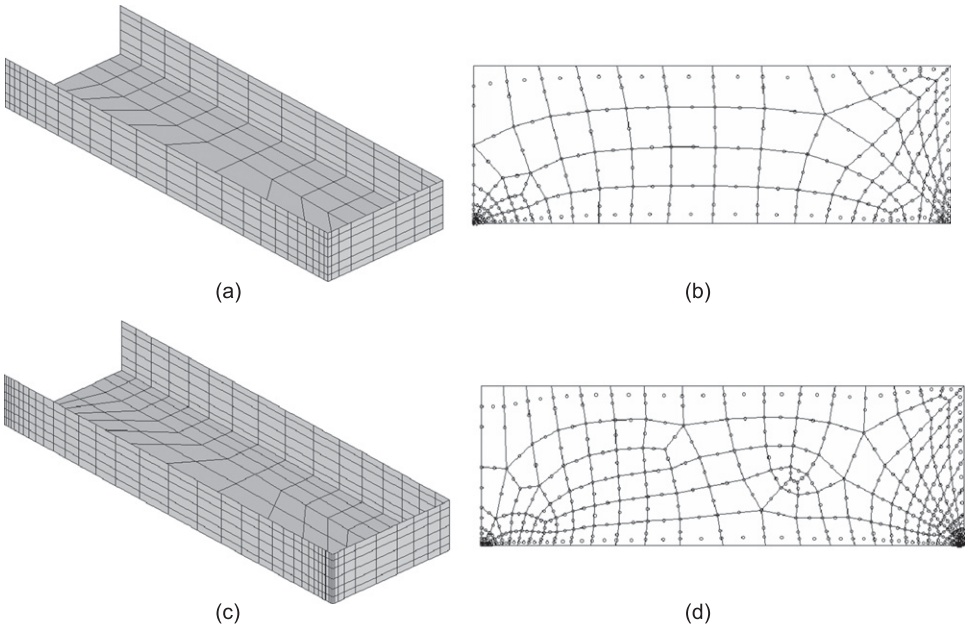

Fig. 2. DIFFRACT meshes for first-order calculation: (a) Mesh 1, body surface, (b) Mesh 1, inner free surface, (c) Mesh 2, body surface and (d) Mesh 2, inner free surface.

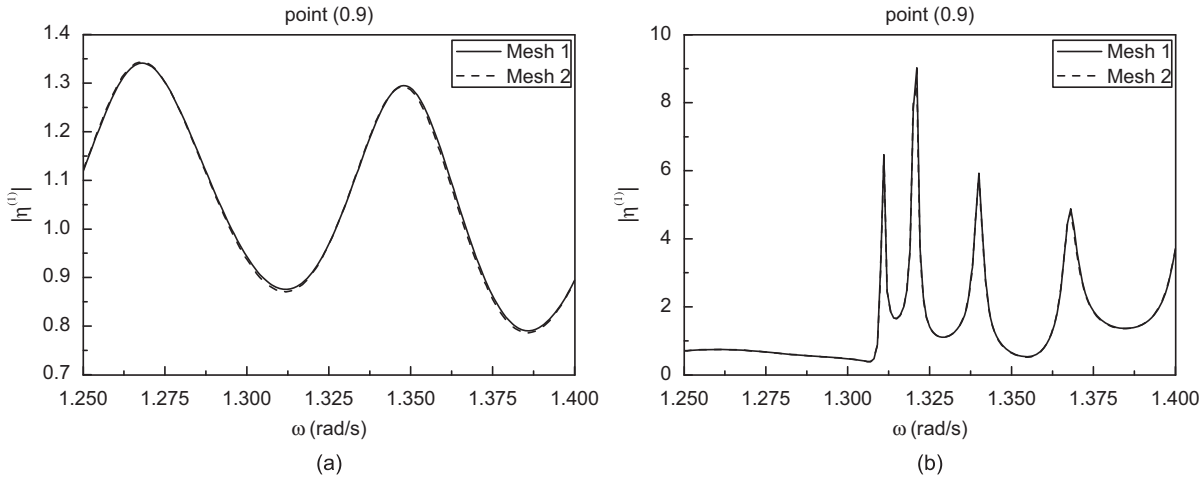

Fig. 3. Free-surface elevation in the gap based on two meshes: (a) head seas and (b) beam seas.

2.3.2. *Influence of spacing on the forces*

The frequencies at which very large forces are predicted on the two boxes, and the associated magnitudes, are strongly dependent on the spacing B, the width of the gap. Fig. 5 compares the beam sea sway and heave forces on boxes 1 and 2 for $B = 4$, 8, 12 and 18 m, with a draft of 16.5 m in each case. The frequency and magnitude of the large peak in the sway force are both seen to increase as the spacing is reduced. The magnitude of the maximum heave force, however, is much less sensitive to spacing.

2.3.3. *Influence of draft on the forces*

Fig. 6 shows the influence of draft on the sway forces on the boxes in beam seas, at a spacing of 18 m. It is to be expected that the sway force increases with draft. But the behaviour is seen to be dominated by resonant type responses,

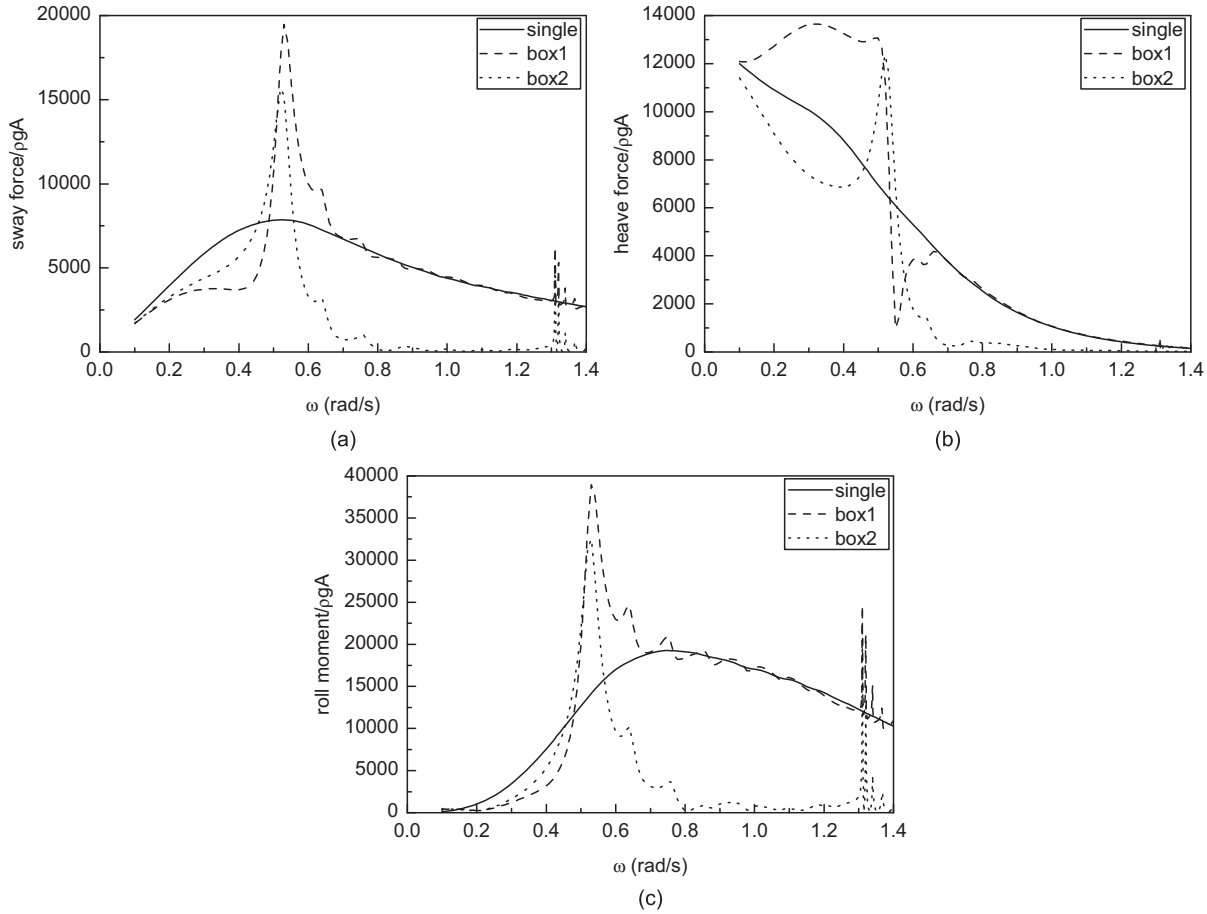

Fig. 4. Wave forces and moment on the boxes: (a) sway, (b) heave and (c) roll.

at frequencies that reduce as draft increases. The peaks also become much narrower banded with increase in draft, an effect which in the potential flow model may be linked to a reduction in damping due to radiated waves, as the flow in the gap becomes more confined.

2.4. First-order motion in beam seas

We next consider the influence of various parameters on the motions of the boxes. Fig. 7 compares the sway and heave response amplitude operators (RAOs) of the two boxes at 18 m spacing with corresponding results for a single box (at a draft of 16.5 m), for the case of beam seas. Most striking is the large increase in resonant heave response of box 1 as a result of interaction effects. In both of the motion responses, secondary peaks are observed about 0.72 rad/s.

The hydrodynamic interactions between the two freely floating boxes in waves yield a rather complex dependence of the motion responses on the incident wave frequency. Resonant free-surface motions excited in the gap in the diffraction problem (fixed boxes) can be superimposed on gap resonances associated with the radiation problem (moving bodies). The heave and roll natural frequencies of the boxes depend on their added masses (including coupling terms), which themselves are strongly influenced by these gap resonances. We therefore also considered the motion responses when one box is fixed and the other is free to respond. Results are shown in Fig. 8 alongside the results when both boxes are freely floating. Again this is for a spacing of 18 m and a draft of 16.5 m, in beam seas. It is of interest to note how the first resonant peak shifts as one or other box is held fixed.

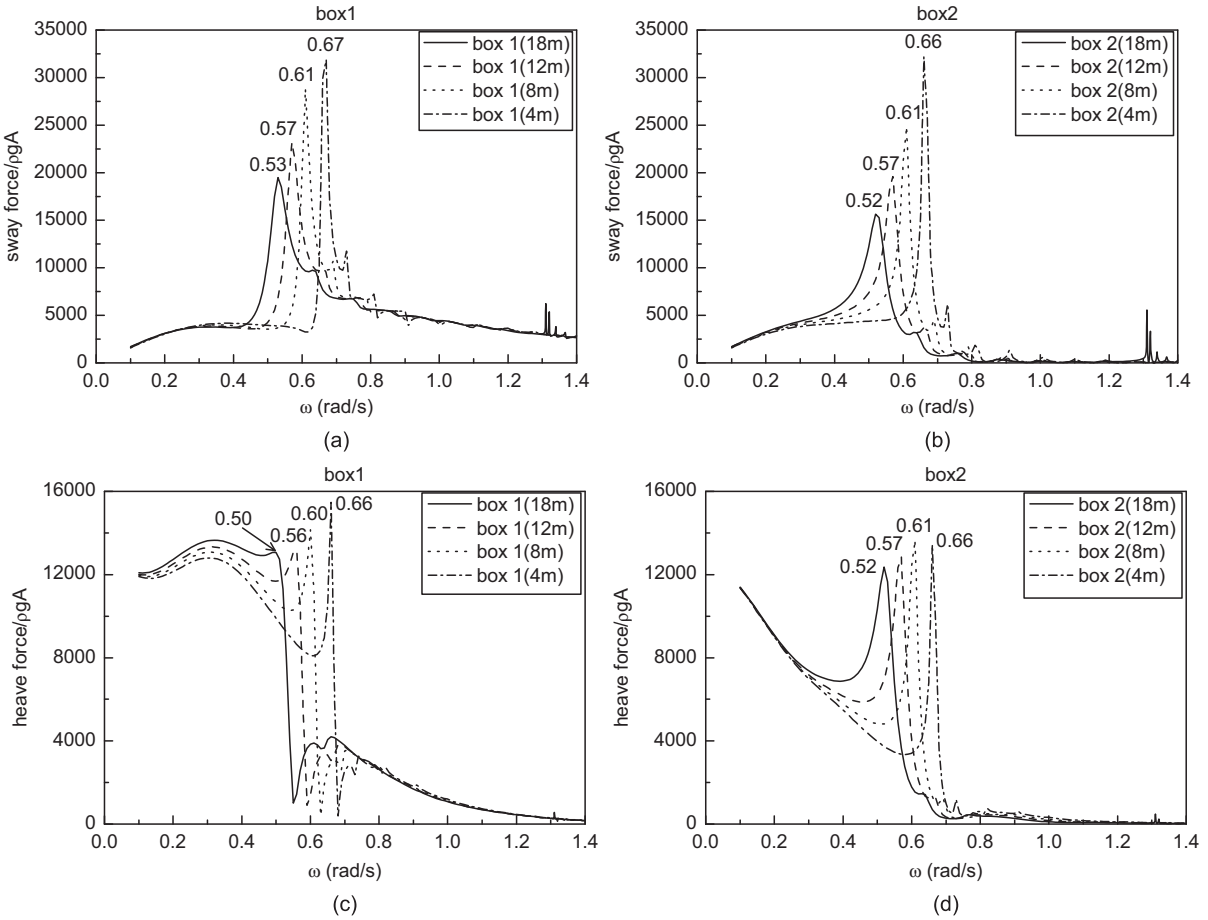

Fig. 5. Dependence of forces on spacing between boxes: sway forces on boxes 1 (a) and 2 (b) and heave forces on boxes 1 (c) and 2 (d).

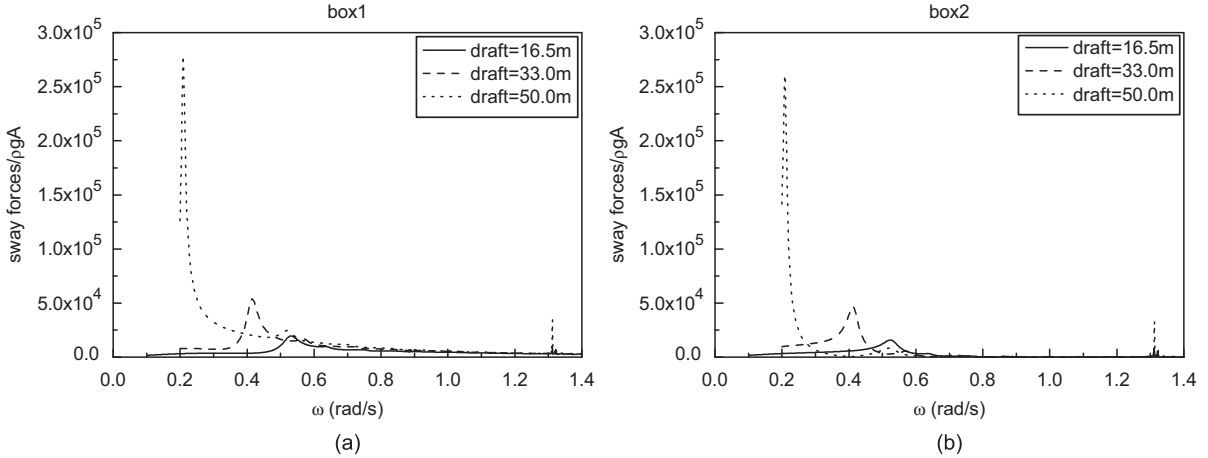

Fig. 6. Dependence of sway force frequency response function on draft: (a) box 1 and (b) box 2.

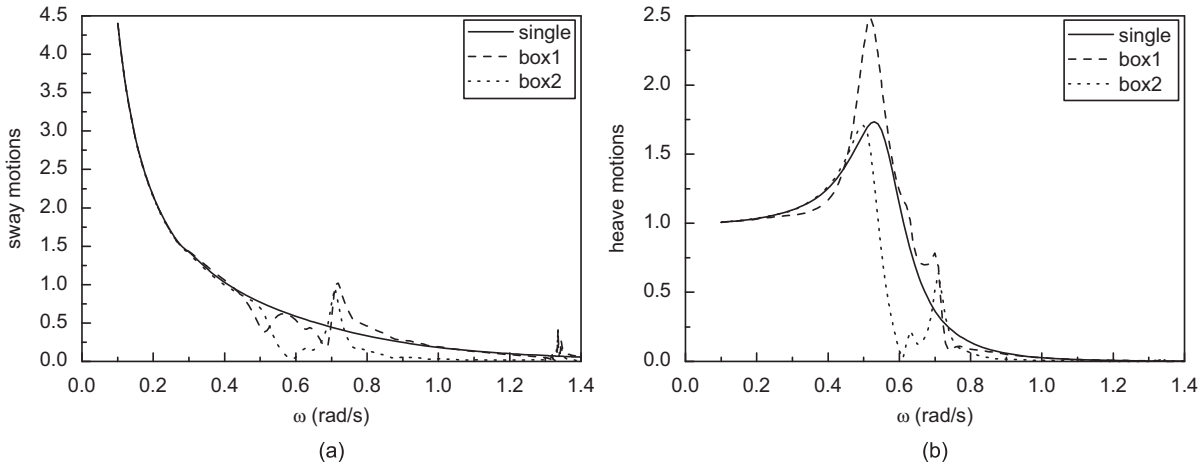

Fig. 7. (a) Sway and (b) heave motion RAOs for the boxes.

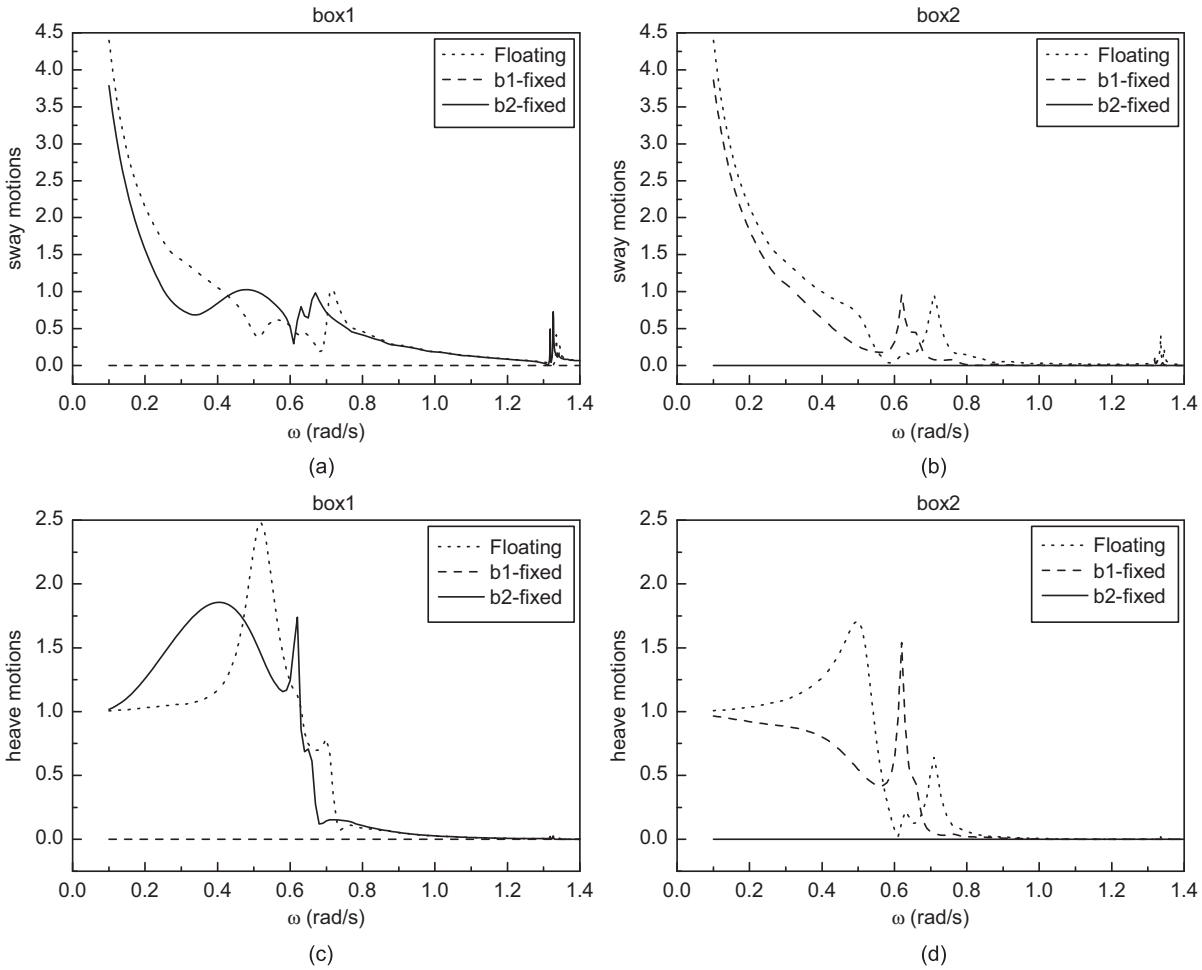

Fig. 8. Effect of motions of one box on the other: sway of boxes (a) 1 and (b) 2; heave of boxes (c) 1 and (d) 2.

2.5. First-order wave elevation in the gap

The motions of the free surface in the gap between the two boxes are now investigated, with parameters varied as before. Results are presented as RAOs of the free-surface amplitude (i.e. per 1 m incident wave amplitude) half-way along the gap, on the wall of box 2 (which is the downwave box in beam seas): this is the point $x = 0$, $y = 9$, in the axes shown in Fig. 1.

2.5.1. Influence of box motions on wave elevation

Fig. 9 shows the free-surface amplitude RAO for cases with both boxes fixed, both freely floating, and one fixed while the other is floating. For clarity, the left-hand figure just shows the first two of these cases, while the right-hand figure shows all. The spacing is 18 m, the draft is 16.5 m, and the boxes are in beam seas.

Similar to the results for the motions in Fig. 8, one can observe that the locations of the peaks shift depending on whether the boxes are fixed or floating. The first resonant peak is now at the same frequency if one or both boxes float freely; however it is at a different frequency if both are fixed. If only one box is free to move, the magnitudes of the peaks are substantially larger than if both are fixed or free (note the different scales in the two diagrams). Very large and very narrow peaks are seen above 1.3 rad/s, which are discussed below.

2.5.2. Influence of spacing on wave elevation

Results are shown in Fig. 10 for the gap elevation in beam seas for the four spacings considered previously, for a draft of 16.5 m. Fig. 10(a) corresponds to both boxes being fixed, while Fig. 10(b) is for both freely floating. As was seen in Fig. 9, there are many more resonant peaks evident in the gap elevation RAOs than in the forces (Fig. 5). The frequencies of the peaks (particularly that at the lowest frequency in each case) depend on the spacing, and the magnitudes increase with decreasing spacing. This is consistent with the results for the forces. The largest peaks are seen to be remarkably high.

2.5.3. Influence of wave direction on the elevation in the gap

Fig. 11(a) and (b) compares, for a spacing of 18 m, the free-surface elevation in the gap in head and beam seas, respectively, with both boxes fixed (still on box 2 half-way along the gap). As in all these results, the DIFFRACT analyses have been undertaken at very closely spaced frequencies, and the locations of the peaks indicated on these plots correspond to the frequencies run that give the highest elevations. It is clear that many of the peaks in head and beam seas are at similar, but not identical, frequencies. The difference is thought to arise because in beam seas the responses are essentially standing waves (to be discussed below), while in head seas these are superposed on a propagating wave (including the effects of diffraction along the length of the gap). The resulting shift in the frequency of the maximum is proportionally greater at the lower frequencies. Another observation from Fig. 11 is that the peaks above 1.3 rad/s in

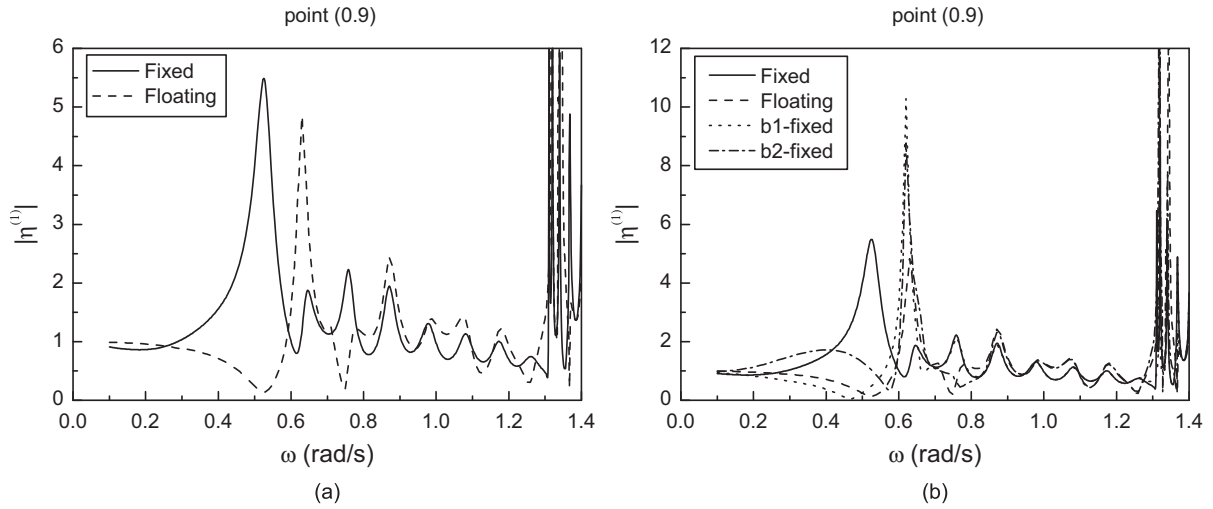

Fig. 9. Effect of box motions on free-surface elevation in the gap in beam seas: (a) both fixed or floating and (b) combinations of fixed and floating (note different scales).

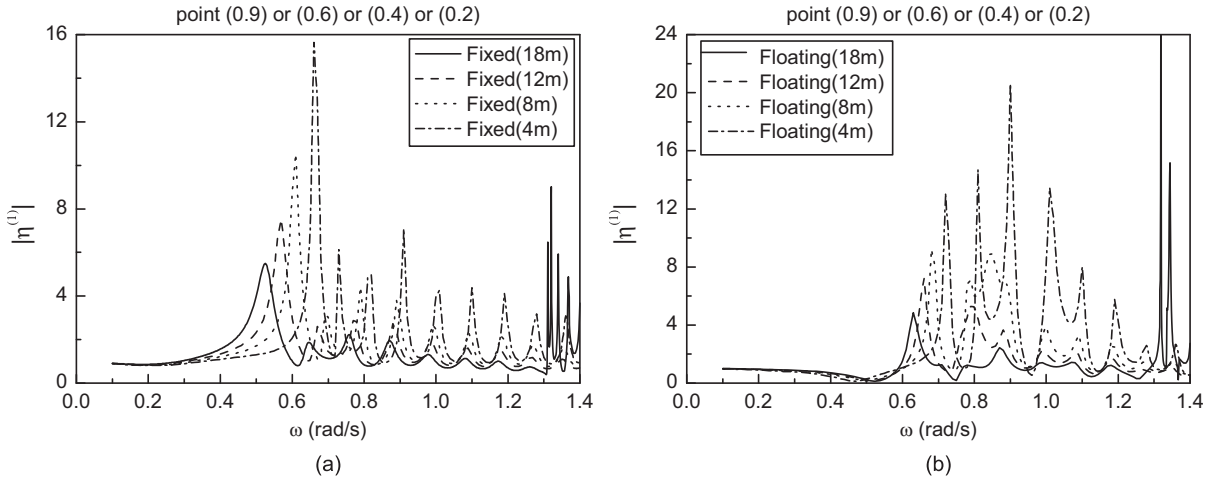

Fig. 10. Effect of spacing on free-surface motion in the gap in beam seas: (a) fixed and (b) floating.

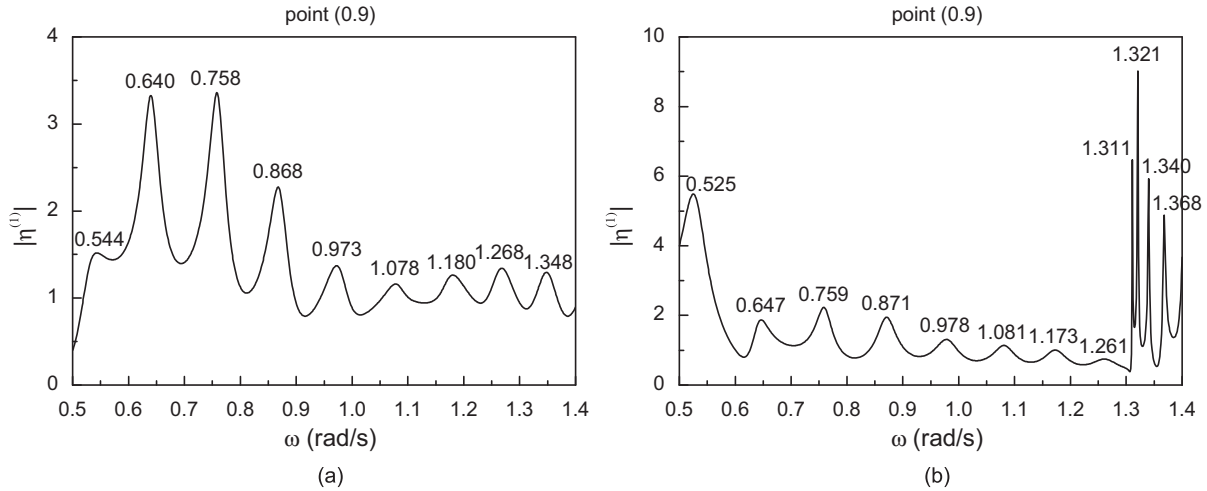

Fig. 11. Free-surface motion in the gap for draft of 16.5 m: (a) head seas and (b) beam seas.

beam seas are absent from the head seas results. It will be shown later that these correspond to a standing wave mode that is antisymmetric across the gap, and therefore cannot be excited in the symmetric case of head seas encountering the two boxes.

Fig. 12 shows for the same geometry the results for five wave heading angles spanning 0–90°. This confirms that there is a gradual transition between the head and beam sea cases.

2.5.4. Influence of draft on the elevation in the gap in head and beam seas

The head and beam sea cases for this arrangement are also studied for two further drafts: 33 and 50 m, in Figs. 13 and 14, respectively. Note that the water depth remains unaltered at 50 m, so for the second case the boxes are bottom-founded. Considering these together with Fig. 11, we see that draft has a major influence on the locations of the resonant peaks in the lower part of the frequency range plotted. In this context it may be noted that a deep water wave of frequency 0.785 rad/s has a wavelength of 100 m. Hence it might be expected that behaviour in these three cases might differ below that frequency, due to the downward reach of the surface wave motion. Furthermore, it is particularly remarkable how much the magnitude of the lowest frequency peak increases in the deeper draft case (note the different vertical scales in these figures). This would appear to be associated with the greater degree of confinement of the flow, as discussed in Section 2.3.3.

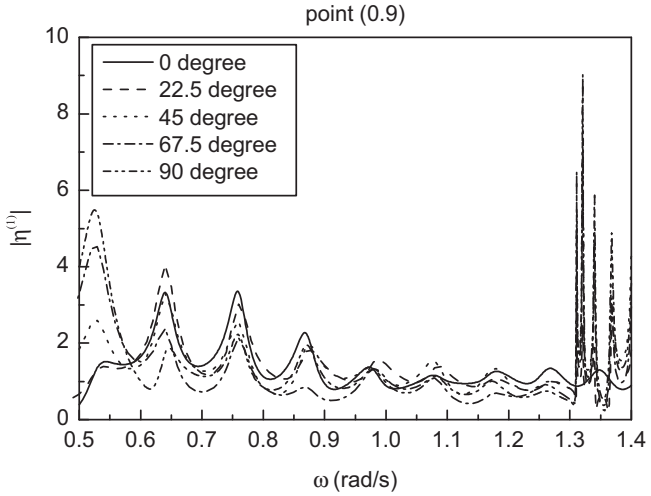

Fig. 12. Influence of wave direction on free-surface elevation in the gap.

2.5.5. Influence of box width on wave elevation

The preceding results have been concerned with identical slender rectangular boxes in a parallel configuration (an idealisation of two tankers side by side). To link this study to other cases of interest, we now extend the numerical modelling using DIFFRACT to a case of two square boxes. We choose a geometry in which the side-length of the square is the same as the length of the rectangular box considered above. Fig. 15 compares the gap elevation when the beam seas encounter square and rectangular boxes of draft 50 m, again in water of 50 m depth. The full frequency range examined is shown in the lowest sub-plot, while the other sub-plots show different frequency ranges on an expanded scale. The increase in box width has a strong effect on the magnitude of the lowest peak, near 0.21 rad/s, and on the first three peaks above 1.3 rad/s.

For the lowest gap resonance with frequency $\omega \sim 0.2$ rad/s, there is a substantial difference in response amplitude for the rectangular ($\times 27$) and square boxes ($\times 12.5$). Since the internal shape of the excited mode within the gap for the two cases is virtually identical, this difference must arise from the local nature of the flow though the ends out into the external regions. Such matching of the internal and external regions is usually done via matched asymptotic expansions, though Lord Rayleigh first solved the free-radiation damping problem of organ pipes in acoustics using a physical matching argument. Howe (2007, Section 6.7, pp. 421–426) gives a recent account of Rayleigh's work in modern notation. Of particular relevance to the comparison of the square and rectangular box solutions in this paper is the difference in damping between an organ pipe with open ends in free-space and one with flanged ends, where each end radiates only out into a half-space. Howe shows that the radiation losses are doubled for the flanged ends, refer to his Eqs. (6.7.7) and (6.7.13), assuming that the flanges extend a significant fraction of a wavelength outwards around the source, as is the case for the square boxes. Although in the water wave problem the ends of the gap radiate free-surface water waves out in 2-D rather than the 3-D acoustic waves for an organ pipe, this dimensional difference does not alter the relative efficiency of radiation from a localised source out into a full- or half-plane. At the lowest resonance near 0.21 rad/s, the half wavelength is 320 m, which greatly exceeds the 46 m beam of the two rectangular boxes. To a first approximation, therefore, the gap between the latter radiates into a full space, while at this frequency the gap between the square boxes radiates into a half-space. Thus, this simple argument would suggest a ratio of 2 in the damping and hence in the peak RAOs in the two cases, which is very close to that shown in Fig. 15 for the lowest resonance. At the next peak around 0.52 rad/s (it is shown below that the second peak corresponds to an $m = 3$ mode along the gap), the half wavelength is only 103 m. It is then plausible to argue that the 46 m width of the rectangular boxes leads to a substantial influence equivalent to finite flanges at the ends of the gap, and therefore to behaviour closer to that of the square boxes, as seen in Fig. 15 at this frequency. For higher modes ($m > 3$) within the gap, the 46 m beam of the boxes is equivalent to ends with flanges extending to infinity, so the radiation damping of these modes for the rectangular and square boxes is very similar.

3. Comparisons with analytical solutions

Understanding of the complex free-surface motions in the gap between two parallel vessels can be facilitated by consideration of two much simpler geometries. We refer to these as the open-ended moonpool and the breakwater with

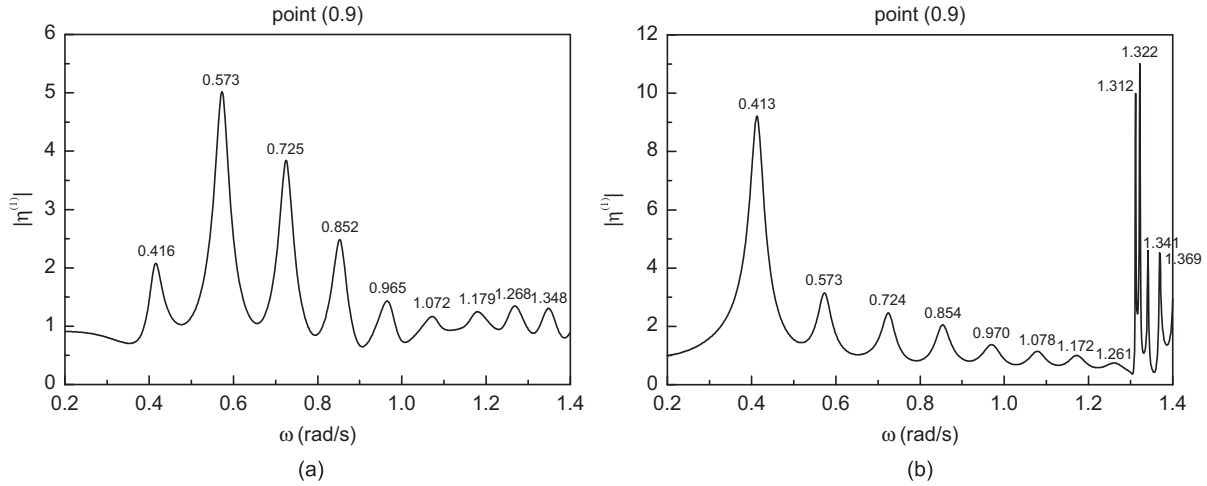

Fig. 13. Free-surface motion in the gap for draft of 33.0 m: (a) head seas and (b) beam seas.

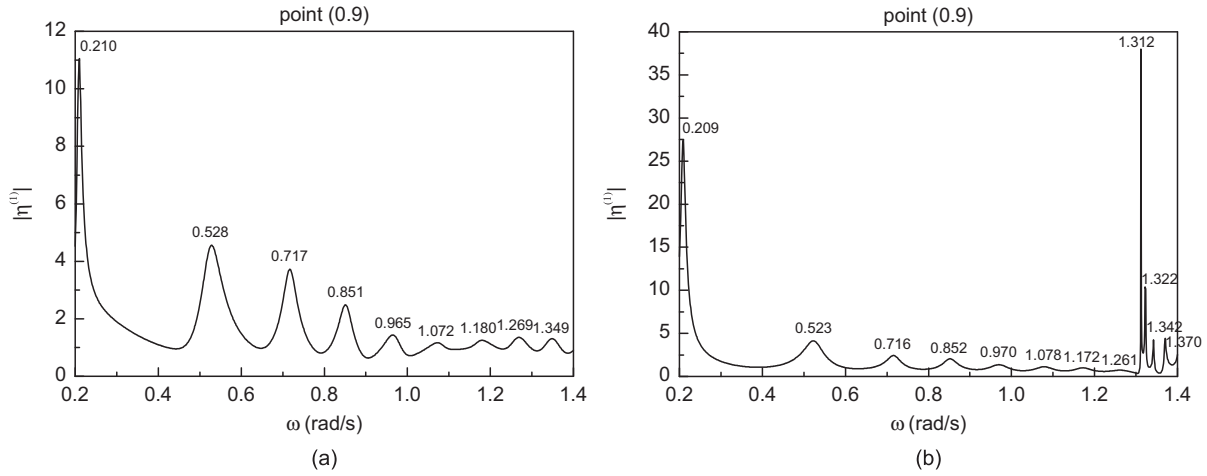

Fig. 14. Free-surface motion in the gap for draft of 50.0 m: (a) head seas and (b) beam seas.

a gap. A semi-analytical solution to the former case yields resonant frequencies and associated eigenmodes, which are remarkably close to those obtained from the boundary element DIFFRACT analysis of the fixed rectangular boxes. The breakwater analysis models vertical structures extending to the seabed, but nevertheless provides useful insight because it leads to simple results for the free-surface responses (in addition to the frequencies of the resonances).

3.1. The open-ended moonpool analysis

This is based on some theory given by Molin et al. (2002), which itself is based on his earlier moonpool analysis (Molin, 2001). The starting point for the moonpool analysis is to consider a rectangular hole in a horizontal plate of infinite extent overlying the fluid. The plate represents a vessel with a moonpool, the draft of the plate being that of the vessel. Based on the assumption of potential flow theory, the flow within the moonpool is expressed in terms of eigenfunction expansions, and matched to the flow below the plate by means of an integral equation. The problem of flow in the gap between two parallel long boxes may be treated similarly. The only essential difference is that for the open-ended moonpool, instead of applying a Neumann boundary condition on the four vertical walls of the closed moonpool, this condition is applied on the two adjacent walls of the parallel boxes with a Dirichlet condition applied at the ends of the gap. This simple model was originally discussed by Newman and Sclavounos (1988), and is found to yield remarkably good approximations to the resonant frequencies of the free-surface motions in the gap.

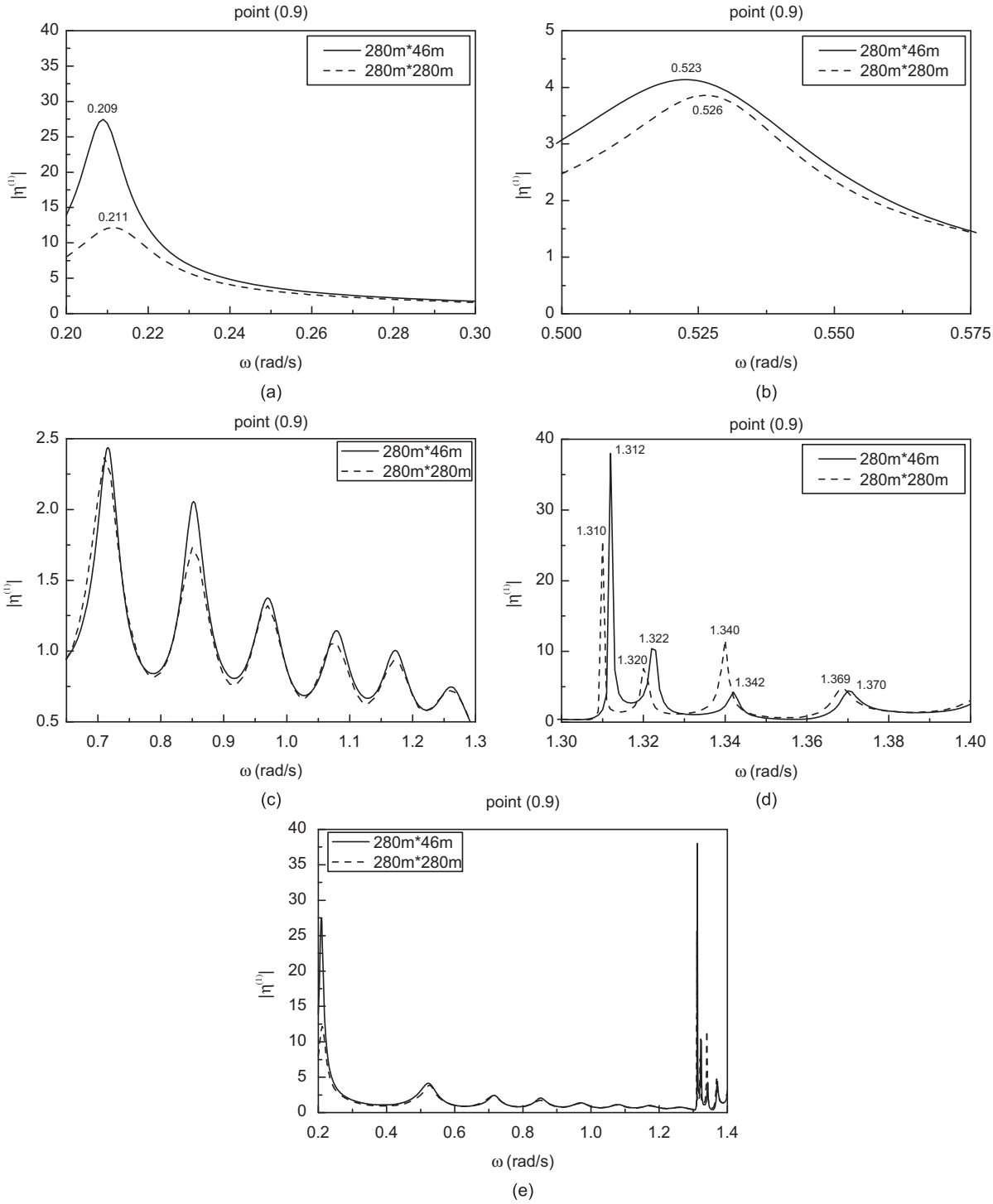

Fig. 15. Comparison of elevation in gap between square and rectangular boxes (plotted over different frequency ranges).

Here we summarise the analysis, more details of which are given in Sun et al. (2008b). As pointed out by Molin (2001), it is easy to see that the velocity potential, Φ, in the half-space is uniquely determined by a Neumann condition at the bottom of the rectangular hole ($z = -H$) and decaying conditions at infinity. The coupling condition

on Φ is then

$$\Phi(x,y,-H,t)=\frac{1}{2\pi}\int_0^L\int_0^B\left(\frac{1}{R}\right)\Phi_z(x',y',-H,t)\,\mathrm{d}x'\mathrm{d}y', \tag{1}$$

where $R=[(x-x')^2+(y-y')^2]^{1/2}$ and the closed moonpool is of length L and breadth B. Here the origin is taken to be at one corner of the moonpool, with z positive upwards from the free-surface. The free-surface condition is

$$\Phi_z-\frac{\omega^2}{g}\Phi=0 \quad \text{on } z=0. \tag{2}$$

Φ satisfies the Laplace equation and the other aforementioned boundary conditions, and it is assumed to be periodic at frequency ω. It can be written in the form

$$\Phi=\sum_{m=0}^{\infty}\sum_{n=0}^{\infty}f_m(x)g_n(y)[A_{mn}\cosh v_{mn}z+B_{mn}\sinh v_{mn}z]\cos\omega t. \tag{3}$$

The functions f_m and g_n are determined by the no-flow boundary conditions on the walls of the closed moonpool, which yield

$$f_m(x)=\cos\lambda_m x, \quad g_n(y)=\cos\mu_n y, \tag{4}$$

where $\lambda_m=m\pi/L$, $\mu_n=n\pi/B$ and $\lambda_m^2+\mu_n^2=v_{mn}^2$. When $m=n=0$, the hyperbolic functions are replaced by $A_{00}+B_{00}\,z/H$. The coefficients A_{mn} and B_{mn} are obtained by imposing the free-surface boundary condition (2) and the coupling condition (1) on $z=-H$. The latter equation is satisfied by using the Galerkin procedure: it is multiplied by $f_{m'}(x)g_{n'}(y)$ and integrated over $(0<x<L,\ 0<y<B)$.

As shown by Molin, this leads to an eigenvalue problem for the resonant frequencies ω_{mn}. He also shows that (unless $H\ll L$ or B) a good approximation may be obtained by ignoring the coupling between the terms m and m', and n and n'. The general form of the solution is then

$$\omega_{mn}^2=gv_{mn}\frac{1+J_{mn}\tanh v_{mn}H}{J_{mn}+\tanh v_{mn}H}, \tag{5}$$

where

$$J_{mn}=\frac{v_{mn}}{2\pi}\frac{\int_0^L\int_0^L\int_0^B\int_0^B(1/R)f_m(x)f_m(x')g_n(y)g_n(y')\mathrm{d}x\,\mathrm{d}x'\mathrm{d}y\mathrm{d}y'}{\int_0^L\int_0^B(f_m(x))^2(g_n(y))^2\,\mathrm{d}x\mathrm{d}y}. \tag{6}$$

The above analysis is equivalent to that developed by Molin (2001) and applied to closed moonpool resonances. As in Molin et al. (2002), we here make a simple modification to enable us to approach the modelling of gap resonances in the open-ended moonpool. Now L is the length of the twin hulls – hence of the gap – and B is their spacing – the width of the gap. The difference from the closed moonpool problem is that instead of another no-flow condition at the ends, we now impose a condition of zero pressure, or $\Phi=0$ at $x=0,\ L$. This of course is a major assumption and simplification of the real physics, the implications of which can be assessed when results from the model are compared with the full 3-D diffraction solution. The consequence of this modification to the moonpool analysis is that we may still use the single-mode approximation of the resonant frequencies given in Eq. (5), but now the modal function $f_m(x)$ is modified to reflect the change of boundary conditions at $x=0,\ L$. Thus we now use

$$f_m(x)=\sin\lambda_m x, \quad g_n(y)=\cos\mu_n y, \tag{7}$$

with the same definitions of λ_m and μ_n as mentioned above.

In the general case of arbitrary m and n, Molin shows that the quadruple integral in Eq. (6) may be reduced to a double integral. In the special case $n=0$ he uses the residue theorem to obtain a simple single integral. For the gap problem, Molin et al. (2002) show that J_{n0} can be written as

$$J_{m0}=\frac{2}{n\pi^2 r}\left\{\int_0^1\frac{r^2}{u^2\sqrt{u^2+r^2}}\left[1+2u+(u-1)\cos(n\pi u)-\frac{3}{n\pi}\sin(n\pi u)\right]\mathrm{d}u-\frac{1}{\sin\theta_0}+1+2r\ln\frac{1+\cos\theta_0}{1-\cos\theta_0}\right\},$$

where $r=B/L$ and $\tan\theta_0=r^{-1}$. For the general case $n>0$ (and in particular $n=1$), we have used a numerical approach as described in Eatock Taylor (2007). Some details are given in Sun et al. (2008b).

This analysis, with $L=280$ m and $H=16.5$ m, has been used to provide estimates of the resonant frequencies in the gap between the two boxes considered above, over the range of spacings $B=4$, 8, 12 and 18 m. The resulting

frequencies in rad/s are given in Table 2 for the first 9 symmetric longitudinal modes in which there is no variation across the gap. These modes are designated (m, n), where $m = 1,3, \ldots, 17$ and $n = 0$. Also shown in this table are the frequencies of successive peaks obtained from the full three-dimensional diffraction analysis (DIFFRACT) of wave elevation at the centre of the gap between the two boxes in beam seas. These peaks are identified in Fig. 11(b) for the case $B = 18$ m. (The missing DIFFRACT result for the mode (17, 0) is discussed below.) Also shown in Table 2 are the corresponding results from the theory and from DIFFRACT for the deeper draft case, $H = 33$ m: these resonant frequencies correspond to the peaks seen in Fig. 13(b). Overall it may be seen that the simple theory gives very close predictions of the resonant frequencies identified from the 3-D diffraction analysis. The agreement is remarkable, given the simplifying geometric assumptions in the theory.

Table 3 shows resonant frequencies as predicted by the theory for the first four longitudinally symmetric $n = 1$ modes, at the same spacings of the barges as considered above and for a draft $H = 16.5$ m. In these modes the free-surface elevation has half a sine wave across the gap of width B. It may be noted that, for each spacing, the frequencies of the $n = 1$ modes do not change much from $m = 1$ to $m = 7$. This may be explained by considering Eq. (5) and the definition of ν_{mn}. Unlike ν_{m0}, which leads to the results in Table 2, the parameter ν_{m1} is dominated by the term μ_1 and so is little influenced by λ_m, because in these cases $B \ll L$. The resonant frequencies may be approximated by $\omega_{m1} \cong \sqrt{(\pi g/B)}$, leading to the results in the right-hand column of Table 3. The results for $B = 18$ m are compared with the estimates from DIFFRACT, indicated in Fig. 11(b) at the right-hand end. Again it is remarkable how closely these values are predicted by the simple theory.

Fig. 16 shows the modulus of wave elevation along the centreline of the gap ($y = 0$), plotted from the middle ($x = 0$) to the open end ($x = 140$ m). The sub-plots correspond to three sample peaks (at $\omega = 0.525$, 0.759 and 1.173 rad/s) of the beam seas RAOs in Fig. 11(b) (for $B = 18$ m, $H = 16.5$ m). These are associated with three modes which are symmetric longitudinally and are uniform in the transverse direction. These plotted results have been obtained from the DIFFRACT analysis, and they are analogous to the (1, 0), (5, 0) and (13, 0) modes, predicted by the simple theory. The principal difference is that they do not reduce to zero at the end of the gap, showing that the Dirichlet condition assumed in the simple theory does not exactly represent the local flow condition at the open end. The wavelengths of the incident waves at the frequencies given in Fig. 16 are about 204, 106 and 44.8 m. The elevation is plotted only along half of the hull length ($0 < x < 140$) because of symmetry. Corresponding to each of these modes it has been confirmed that the transverse variation of the elevation (along $x = 0$) is negligible, confirming that all these are indeed of type $(m, 0)$.

Table 2
Resonant frequencies for elevation in gap between two boxes at different spacings: $n = 0$ modes.

H (m)	B (m)	Mode	1,0	3,0	5,0	7,0	9,0	11,0	13,0	15,0	17,0
16.5	4	Theory	0.65518	0.73141	0.81856	0.91491	1.01304	1.1087	1.20005	1.28663	1.36859
		DIFFRACT	0.66	0.73	0.82	0.91	1.01	1.10	1.19	1.28	1.361
16.5	8	Theory	0.59628	0.69651	0.79824	0.90369	1.00710	1.10564	1.19851	1.28586	1.36821
		DIFFRACT	0.61	0.69	0.79	0.89	0.99	1.09	1.18	1.27	1.355
16.5	12	Theory	0.55687	0.67400	0.78586	0.89723	1.00385	1.10405	1.19774	1.2855	1.36804
		DIFFRACT	0.57	0.67	0.77	0.88	0.99	1.09	1.18	1.27	1.351
16.5	18	Theory	0.51567	0.65126	0.77398	0.89132	1.00100	1.1027	1.19711	1.28521	1.36791
		DIFFRACT	0.525	0.647	0.759	0.871	0.978	1.081	1.173	1.261	
33.0	18	Theory	0.44534	0.59864	0.74671	0.87865	0.99535	1.10021	1.19602	1.28473	1.36769
		DIFFRACT	0.413	0.573	0.724	0.854	0.970	1.078	1.172	1.261	

Table 3
Resonant frequencies for elevation in gap between two boxes at different spacings: $n = 1$ modes.

B (m)	Mode	1,1	3,1	5,1	7,1	$\sqrt{(\pi g/B)}$
4	Theory	2.77546	2.77659	2.77885	2.78223	2.77532
8	Theory	1.96285	1.96605	1.97239	1.98179	1.96245
12	Theory	1.60233	1.60915	1.62062	1.63739	1.60233
18	Theory	1.31354	1.32356	1.34338	1.37184	1.30830
	DIFFRACT	1.311	1.321	1.340	1.368	

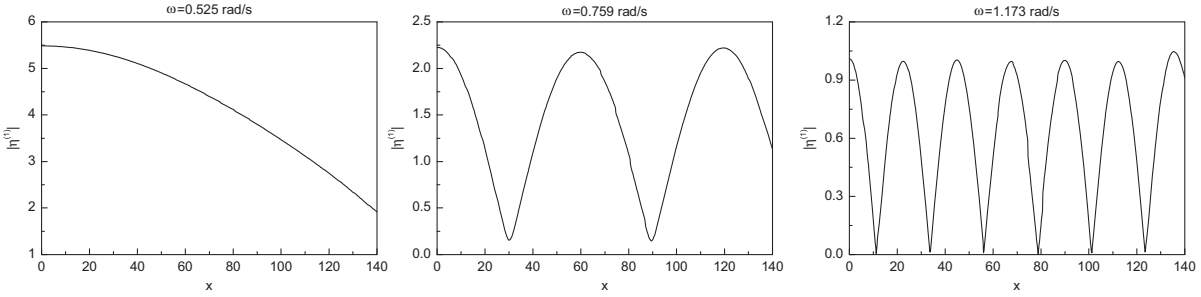

Fig. 16. Wave elevation along 18 m gap in beam seas, at 3 peak frequencies ($n = 0$ modes).

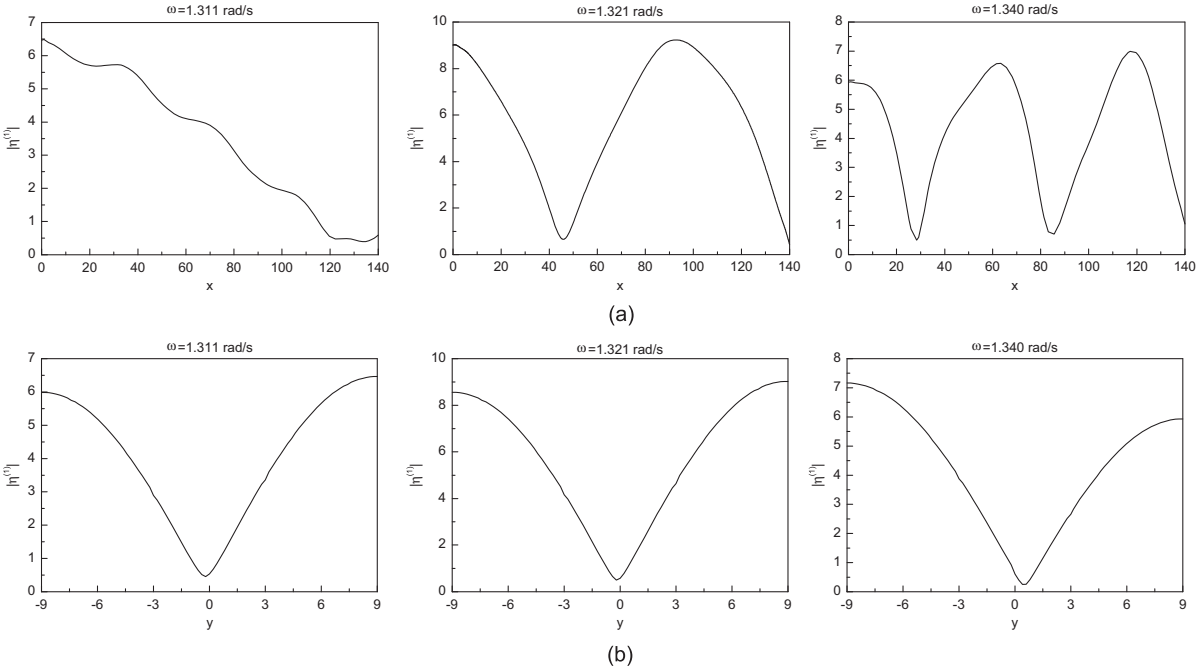

Fig. 17. Wave elevation in 18 m gap in beam seas, at 3 peak frequencies ($n = 1$ modes): (a) variation along gap and (b) variation across gap.

The elevations obtained from the DIFFRACT analysis at the frequencies exciting the first three longitudinally symmetric $n = 1$ modes in beam seas are shown in Fig. 17: these correspond to mode (1, 1) at $\omega = 1.311$ rad/s, mode (3, 1) at $\omega = 1.321$ rad/s and mode (5,1) at $\omega = 1.340$ rad/s. The variation along the gap of the elevation on the sidewall of box 2 ($y = 9$ m) is shown in Fig. 17(a), and that across the gap at the centreline ($x = 0$) is shown in Fig. 17(b). It is clear that these modes are antisymmetric in the transverse direction ($n = 1$ corresponding to one-half-wave across the gap), so they cannot be excited in head seas. This is clear from the RAOs in Fig. 11. It appears that within the narrow frequency band 1.31–1.37 rad/s the diffraction analysis predicts the occurrence of five separate resonances: in beam seas at the three (m, 1) frequencies mentioned above and the (7, 1) mode at 1.368 rad/s and in head seas at 1.348 rad/s (corresponding to the (17, 0) resonant standing wave mode superimposed on a wave propagating along the gap). The (17, 0) resonance cannot be distinguished in the beam sea case, because it is swamped by the neighbouring (5, 1) peak. This is the reason for the lack of a DIFFRACT result for (17, 0) in Table 2. The response in Fig. 17(a) at 1.311 rad/s is clearly dominated by the (1, 1) resonance with a half sine wave over the full length of the gap, but it is interesting to observe the contamination by what is presumably a contribution from the (m, 0) mode at a neighbouring resonant frequency (possibly (15, 0) at 1.261 rad/s). This effect is not clearly seen in the higher (m, 1) modes, probably because the next longitudinal mode (17, 0) could be expected to make a rather small contribution. The general conclusion from

these plots of elevations as predicted by DIFFRACT is that they are clearly consistent with the sinusoidal modes, longitudinally and transversely, as predicted by the simple theoretical model; but there are minor differences in behaviour at the ends of the gap.

3.2. Analysis for the breakwater with a gap

The previous simple theory in Section 3.1 provides resonant frequencies and modes of free-surface response in the gap, but yields no information about the absolute magnitude of response at any point. It only solves the homogeneous problem, yielding a radiating wave solution of unspecified amplitude. By simplifying the problem still further, we can investigate a case for which the complete forced response solution can be very simply formulated. This is the case of a breakwater pierced by a narrow canal, discussed by Mei (1983).

Consider the two fixed rectangular boxes (again of length L) now extending down to the seabed. The case of excitation by beam seas is then related to the problem of waves at a breakwater of infinite length, in which is cut a rectangular channel of length $L/2$ and width B (see Fig. 18). The solution to this problem is given by Eq. (6.18) on page 203 of Mei (1983). Reformulated in terms of the variables in our problem, this gives the free surface magnification as

$$\frac{|\eta(0)|}{A} = \frac{1}{\cos(kL/2) + (kB/\pi)\sin(kL/2)\ln(\gamma kB/\pi e) - i(kB/2)\sin(kL/2)},$$

where A is the amplitude of the incident wave (beam on to the two blocks). In the equation, $e = \exp(1)$ and γ is defined from Euler's constant by $\ln \gamma = 0.5772157$. This solution is independent of water depth.

The solution is obtained by matched asymptotics, and is based on the assumption that the width of the gap is much less than the wavelength. At the end of the gap the solution is taken as that for a simple source. Away from the end, the solution in the gap is two-dimensional. It is therefore potentially useful only for the $n = 0$ modes. The theory is also based on the channel being inserted into an infinitely long wall: its use in modelling the gap between the two cuboidal blocks will therefore depend on their relative width W.

Fig. 19 compares the predictions from this theory with DIFFRACT results for square blocks of dimensions $L = W = 280$ m. The water depth is 50 m and the width of the gap is $B = 18$ m. The modulus of the dimensionless elevation predicted by DIFFRACT half-way along the inside face of the downwave block ($x = 0$, $y = 9$ m) is plotted over the frequency range ($0 < \omega < 1.4$ rad/s) in Fig. 19(e).

Expanded plots over parts of this range, selected to cover all of the peaks, are shown in Fig. 19(a)–(d). These are the same results as plotted in Fig. 15 and compared there with the corresponding results for barges of width $W = 46$ m. These results are compared in Fig. 19 with those from the simple theory. It is clear that the locations of the peaks agree very closely, as do the amplitudes of the responses up to around 0.9 rad/s. It may also be seen that the last four peaks in this range (i.e. those lying in $1.3 < \omega < 1.4$ rad/s) are not represented in the simple solution. This of course is because they correspond to $n = 1$ modes, which are absent from the simple theory.

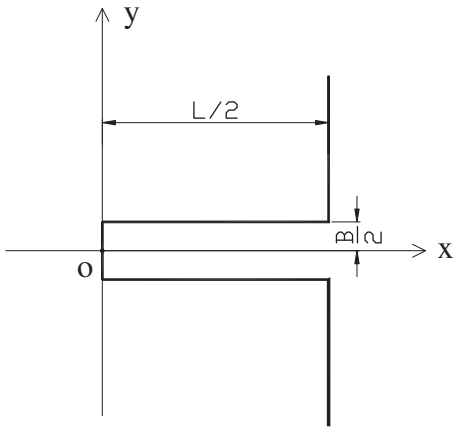

Fig. 18. Sketch of channel in infinite breakwater.

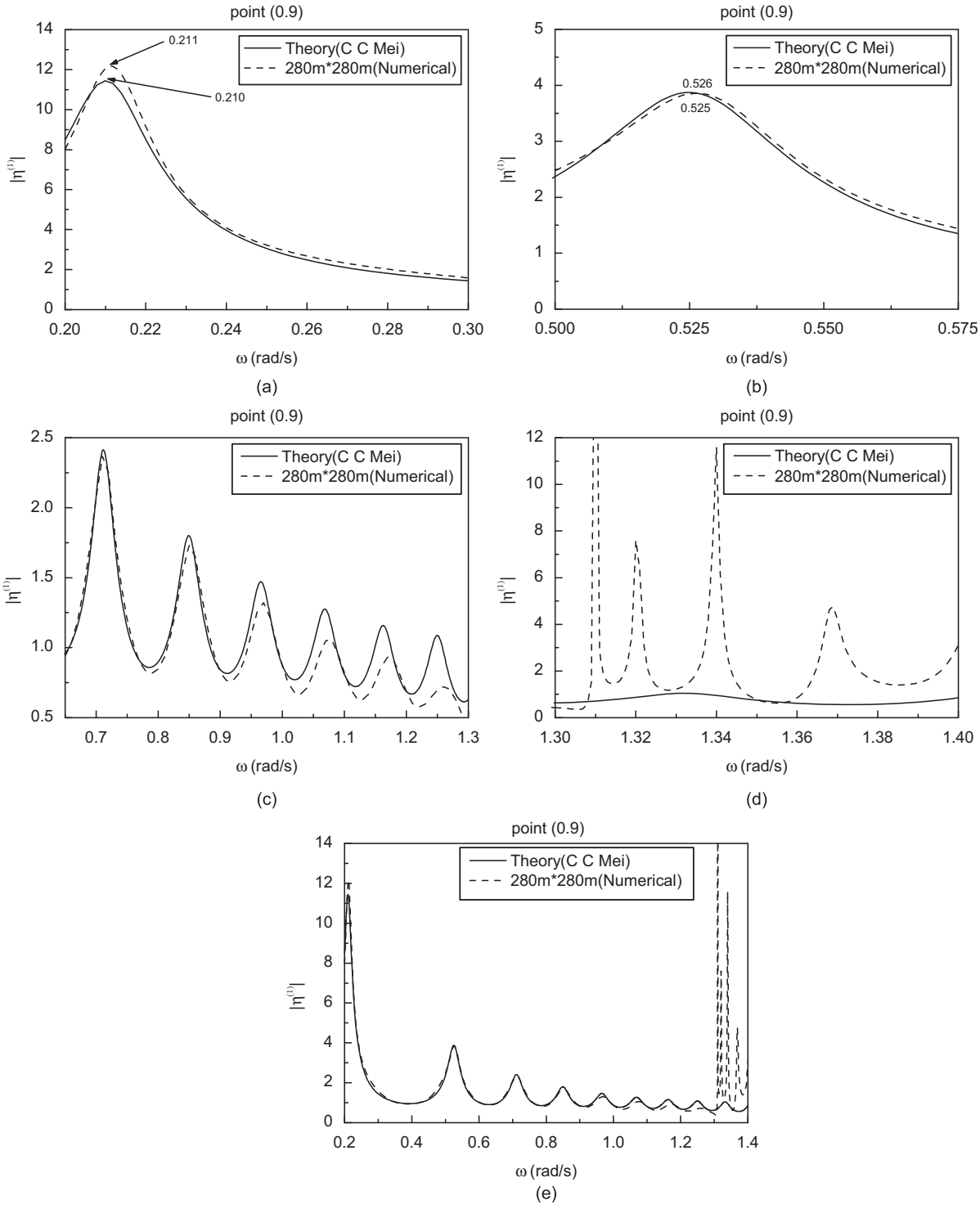

Fig. 19. Comparison of predictions of wave elevation by simple theory of Mei (1983) for a channel in a breakwater and numerical prediction for square boxes: (a–d) sub-plots over different frequency ranges and (e) the complete range 0.2–1.4 rad/s.

All these comparisons with analytical solutions provide confidence in the 3-D boundary element code DIFFRACT. They also yield understanding of the very strong resonant effects identified in the potential flow analysis of two parallel vessels in waves.

4. Second-order behaviour

4.1. Analysis of forces on fixed boxes in beam seas

The investigation of the two-box configuration is next extended to consider forcing and free-surface elevation at second order. The aim here is first to confirm the expectation that gap resonances can cause large hydrodynamic responses due to second-order effects, when the incident wave frequency is half of the frequency of the first-order resonances. Secondly, the second-order diffraction analysis provides an indication of just how large are the ideal flow predictions of such second-order effects.

First it may be recalled that second-order forces in a Stokes expansion can be separated into two components. One of these is based on products of pairs of terms resulting from the first-order analysis: the first-order potential, the first-order force, the first-order motion response (for moving bodies), etc. These may be designated "quadratic" terms, and identified with the subscript "q". The other component arises from the second-order potential itself, which is the solution at second order of the nonlinear boundary value problem expanded to terms of second order. The subscript "p" is used to identify these terms. The boundary value problem for the second-order potential involves a non-homogeneous free-surface boundary condition, which in turn, in the integral equation formulation of the frequency domain problem, leads to an integral over the complete free surface. It is this integral which leads to the computational difficulty of second-order diffraction analysis. The approach used here involves a numerical integration over the 2-D region in the vicinity of the bodies, coupled with a line integral of individual angular harmonics beyond the circular boundary of that region. The line integral itself is divided into two parts: that furthest from the bodies being approximated through asymptotic expansions of the various terms in the free-surface integral. Crucial to the accuracy of the computation is the discretisation of the near-field 2-D region of the free surface. In DIFFRACT use is made of a mesh of triangular and quadrilateral panels, with the variables defined in terms of nodal values just as in the linked boundary element representation of the body surfaces. Gaussian quadrature is used to integrate over each panel. The key parameters are the sizes and shapes of the panels, and the extent of the region (as defined by the radius of its outer boundary). These aspects of convergence are considered next.

In the second-order analysis of the two boxes, as at first order, use is made of two planes of symmetry. It is therefore only necessary to discretise explicitly one quadrant of the free surface. As shown in Fig. 20, four meshes were used, with outer radii of 400, 700 and 1100 m. The first two of these were used initially to calculate second-order forces on a single box. The 1100 m radius mesh was used for the two-box case, with two average sizes of panel on the free surface: 30 and 12 m, respectively. It may be seen that the meshes are designed to be finer near the body surface and particularly near the sharp corner, where in theory there would be a singularity in the tangential flow velocity. Fig. 21 shows the second-order potential contribution to the sway force on a single box in beam seas, based on the free-surface meshes in Fig. 20(a) and (b). The average panel size in each case is 12 m. The results are plotted over the frequency range $0.5<\omega<0.7$ rad/s, which is relevant to the comparisons below. It may be seen that the two lines, corresponding to the outer radii of 400 and 700 m, are virtually indistinguishable. Fig. 22 shows the second-order potential contribution $F_{yp}^{(2)}$ to the sway force on each of the two boxes spaced 18 m apart. This is plotted over the upper part of the frequency range mentioned above, with the forces in Newtons divided by $\rho g A^2$. It is of interest in the context of convergence because accuracy of the free-surface integral becomes progressively more difficult to achieve as the frequency increases. The results have been obtained using the meshes equivalent to those in Fig. 20(c) and (d), both with an outer radius of 1100 m. The average panel size indicated in the legends (30 and 12 m) refers to panels within the inner circular boundary, but away from the immediate vicinity of the boxes. Much smaller panels are used in the gap, and around the hulls where the nodes match those on the hulls at the waterline. At this spacing between the boxes there are very significant oscillations in the plots, captured by using a very fine frequency resolution in the calculations. While the force on the downstream box 2 calculated with the 30 m average size panels appears close to the converged result, this is not the case for the second-order force on box 1. The 12 m average element mesh size is used for the subsequent calculations.

Next the force on a single box by itself is compared with the forces on boxes 1 and 2 when separated by a gap of width 18 m. Fig. 23 shows the contribution of the quadratic terms to the second-order sway force in beam seas over the frequency range $0.5<\omega<0.7$ rad/s. Within this frequency range, there is very little variation in the force on the single box; however for the two boxes the interactions cause substantial frequency dependence from the products of the

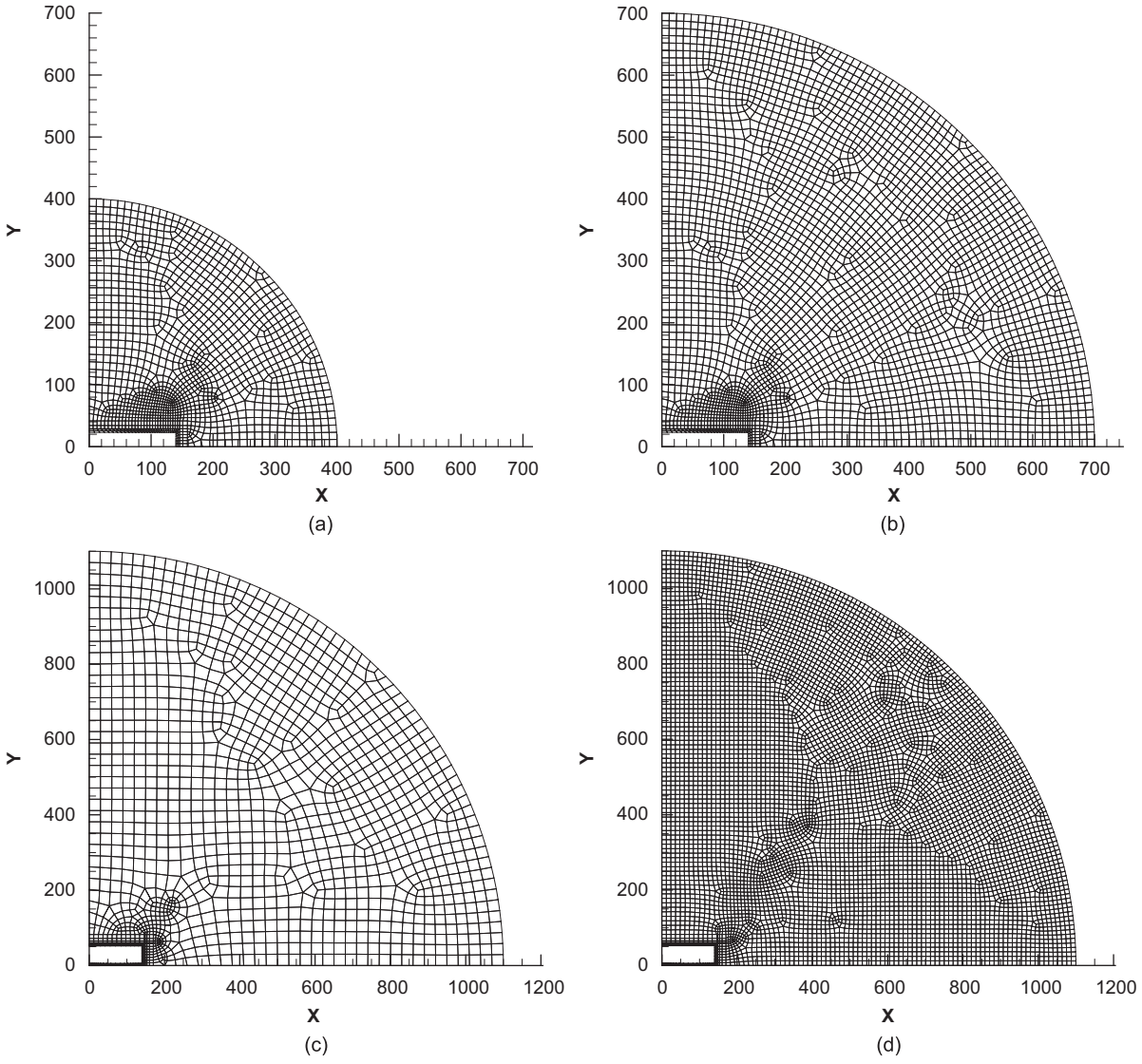

Fig. 20. Free-surface meshes for second-order calculations for boxes using two planes of geometric symmetry: (a, b) for a single box and (c, d) for two boxes.

first-order components. The contribution from the second-order potential in this case is shown in Fig. 24. The left-hand plot shows the frequency range $0.5<\omega<0.7$ rad/s (as in Fig. 23); a zoom into the range $0.63<\omega<0.70$ rad/s is shown in the right-hand plot. The latter shows peaks for the two-box case at around 0.655, 0.660, 0.670 and 0.684 rad/s. These are half the frequencies of the $n=1$ peaks shown in Fig. 11(b), as expected from second-order theory for this spacing. The total sway force on the boxes is shown in Fig. 25. It may be noted that even though the quadratic and potential contributions have broadly similar shapes in Figs. 23 and 24 in the range up to 0.65 rad/s (where $n=1$ modes become excited), they are roughly out of phase. Hence while both contributions have large peaks around 0.525 rad/s (linked to the (1,0) mode), the net effect is only a small peak in Fig. 25. The lowest two $n=1$ mode contributions due to the second-order potential are seen to dominate the behaviour.

4.2. Second-order elevations in the gap between fixed boxes in beam seas

In order to illustrate how second-order potential effects excite peaks at half the frequencies of first-order peaks, it is instructive to consider the case of 18 m spacing between the boxes, of draught 16.5 m. As seen in Fig. 11(b), first-order

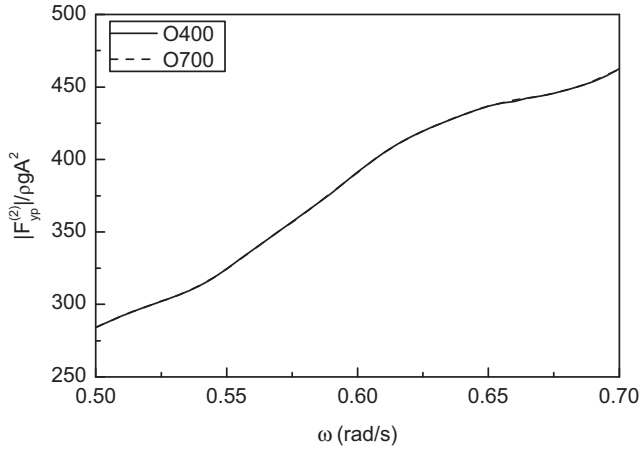

Fig. 21. Second-order potential contribution to sway force on a single box.

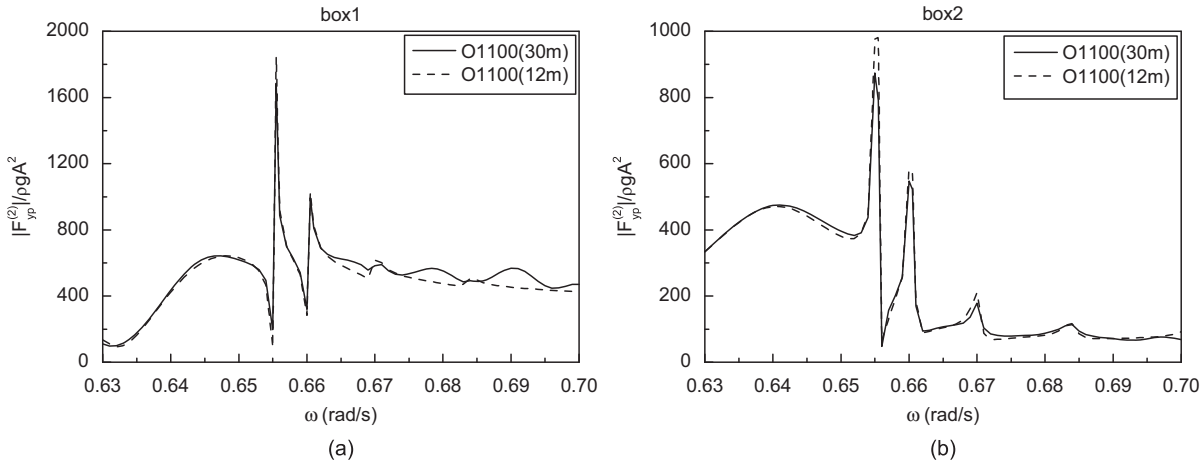

Fig. 22. Second-order potential contributions to sway forces on boxes using two different meshes for 18 m spacing: (a) box 1 and (b) box 2.

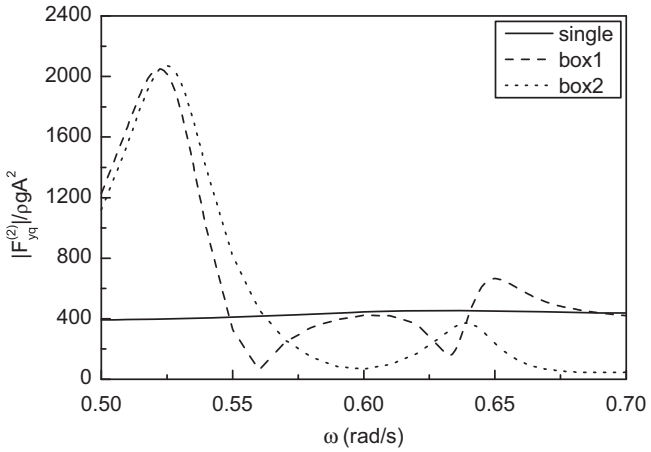

Fig. 23. Quadratic contributions to second-order horizontal forces on boxes (18 m spacing).

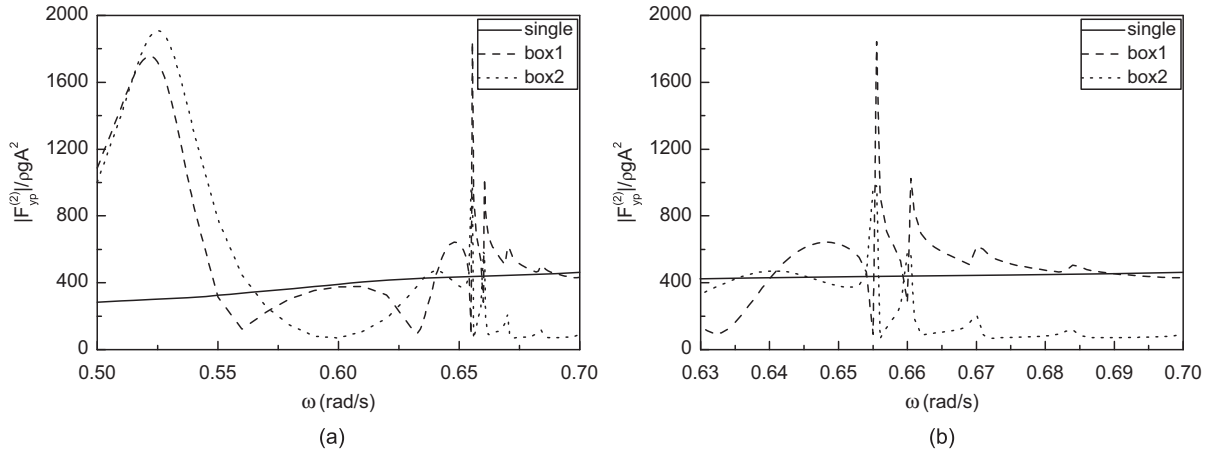

Fig. 24. Potential contributions to second-order horizontal forces on boxes (18 m spacing, plotted over different frequency ranges).

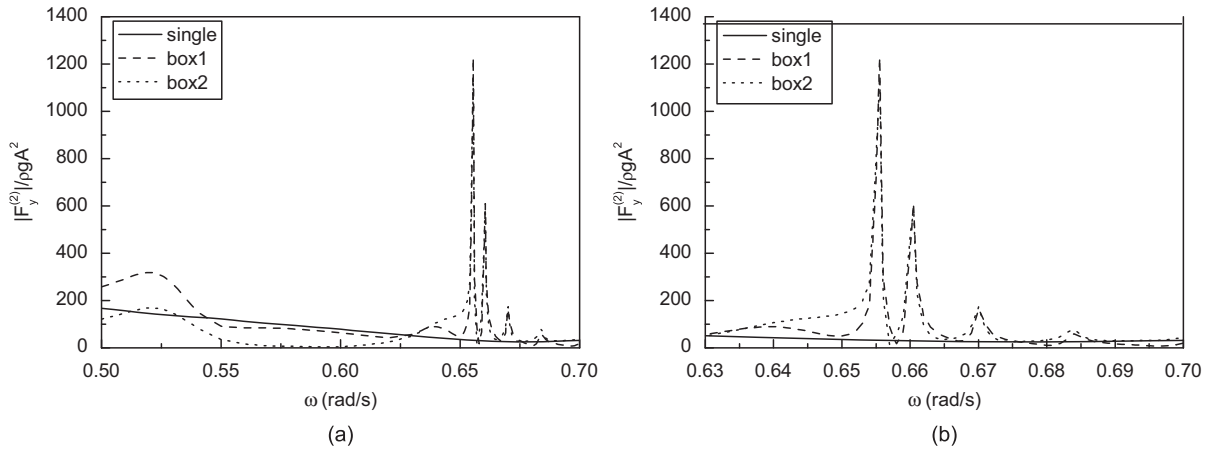

Fig. 25. Total second-order horizontal forces on boxes (18 m spacing, plotted over different frequency ranges).

resonant motions in the gap have been identified in the frequency range 0.5–1.4 rad/s. The results have been interpreted in the light of the simple analysis in Section 3.1, leading to the identification of $n = 0$ and $n = 1$ modes within this range of frequencies. Of particular note is that the lowest four $n = 1$ modes, tightly spaced in the range 1.31–1.37 rad/s, are at approximately twice the frequency, 0.65 rad/s, of the (3, 0) mode. It is of interest, therefore, to seek evidence of multiple modes responding simultaneously to this configuration, due to the combination of first- and second-order excitations.

Fig. 26 shows the magnitude of the wave elevation at the centre of the gap, over the range $0.5 < \omega < 0.7$ rad/s and per 1 m incident wave amplitude. The quadratic and potential terms are shown separately, along with the total. Peaks in the quadratic term are found at 0.526 and 0.647 rad/s, corresponding to those seen at or near these frequencies in Fig. 11. The potential term also shows peaks around these first-order resonant frequencies. The other peaks in the potential term, which can only be identified by plotting at very close frequency spacing, are at or near 0.6555, 0.6605, 0.670 and 0.684 rad/s. These are precisely half the frequencies of the $n = 1$ modes seen in Fig. 11(b). Such results suggest that while the (3, 0) mode is excited by first-order effects at 0.647 rad/s, the (3, 1) mode is probably excited by second-order effects at 0.6605 rad/s.

Examination of the distribution of the wave amplitude along and across the gap provides the evidence that the (3, 0) and (3, 1) modes are indeed excited simultaneously at 0.6605 rad/s. The plots for this frequency are shown in Fig. 27, illustrating the spatial variation of linear, second-order quadratic and second-order potential terms. For each term the distribution along the gap ($0 < x < 140$ m, $y = 9$ m) is seen to correspond to the $m = 3$ mode. Across the gap ($x = 0$, $-9 < y < 9$ m) the linear and quadratic terms are constant, i.e. $n = 0$, and the potential term corresponds to a half sine

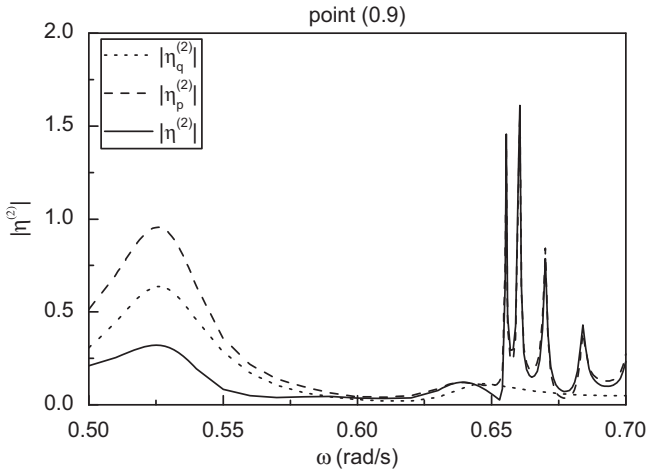

Fig. 26. Components of second-order elevation on box 2 half-way along the gap (quadratic, potential and total).

wave, $n = 1$. The quadratic term is in this case much smaller than that due to the second-order potential, but its behaviour is very clear. The second-order potential term as scaled here is very similar to the linear component. As however these are defined as amplitudes for an incident wave of unit amplitude, it is apparent that in larger waves the second-order resonant response is predicted to be very large indeed.

5. Conclusions

Results have been presented in this paper which shed light on some rather sensitive hydrodynamic effects arising when two vessels are parallel and closely spaced. The vessels might be at a critical stage in an approach manoeuvre, or moored at their closest operational spacing (taken here to be 4 m). Simple linear theory predicts very strong hydrodynamic interaction effects between the two structures, which may be associated with the excitation of standing waves in the gap between them. This can affect wave forces, motion responses and local free-surface elevations, leading to large peaks in response amplitude operators and large magnifications of the forces and responses arising in the case of isolated bodies. These effects have been investigated in the present study. The numerical analysis has been undertaken using the potential flow diffraction code DIFFRACT.

The results show that the frequencies and magnitude of the peaks in the forces are in general strongly dependent on the spacing, i.e. on the width of the gap. The heave forces, however, are less affected than sway. With increasing draft, the peaks in the force RAOs increase, and they occur at lower frequencies. At the closest spacing, the largest sway force is predicted (in the absence of any viscous effects) to be at least 4 times the maximum sway force on a single box in isolation. It occurs at a wave period of roughly 9 s.

Investigation of the motion responses suggests that heave is strongly affected by the interactions, as well as the other motions. The peak in the RAO for heave in beam seas, corresponding to the heave resonance, was found to be about 2.5 for each of the spacings examined, as compared with 1.75 for a box in isolation. If one of the closely spaced boxes is fixed and the other floats freely, the motions are substantially different from the case when both boxes are free.

The RAOs for wave elevation at the centre of the gap display many more large peaks than observed in the forces and motion responses. The locations of the peaks are strongly dependent on whether one or both boxes are fixed or freely floating. The location of the peaks for the fixed case has been investigated through the use of some simple theory for an open-ended moonpool, which provides remarkably good predictions of the values from the full diffraction analysis using DIFFRACT. The simple theory also sheds light on the nature of the standing waves set up in the gap. It supports the distinction between a set of lower frequency modes, which are constant in amplitude across the gap, and closely spaced higher frequency modes, which are antisymmetric across the gap (and therefore not excited by head seas, propagating parallel to the slender gap). These higher frequency peaks are in general narrow and of larger amplitude than those at lower frequency. The lowest frequency antisymmetric mode was predicted at 4.8 s, and this corresponds to the largest spacing considered (18 m). Examination of the free-surface elevation in the gap for different wave heading angles showed a gradual transition of behaviour between head seas and beam seas. The principal difference is that as the incident angle tends towards the head sea case, the effect of the

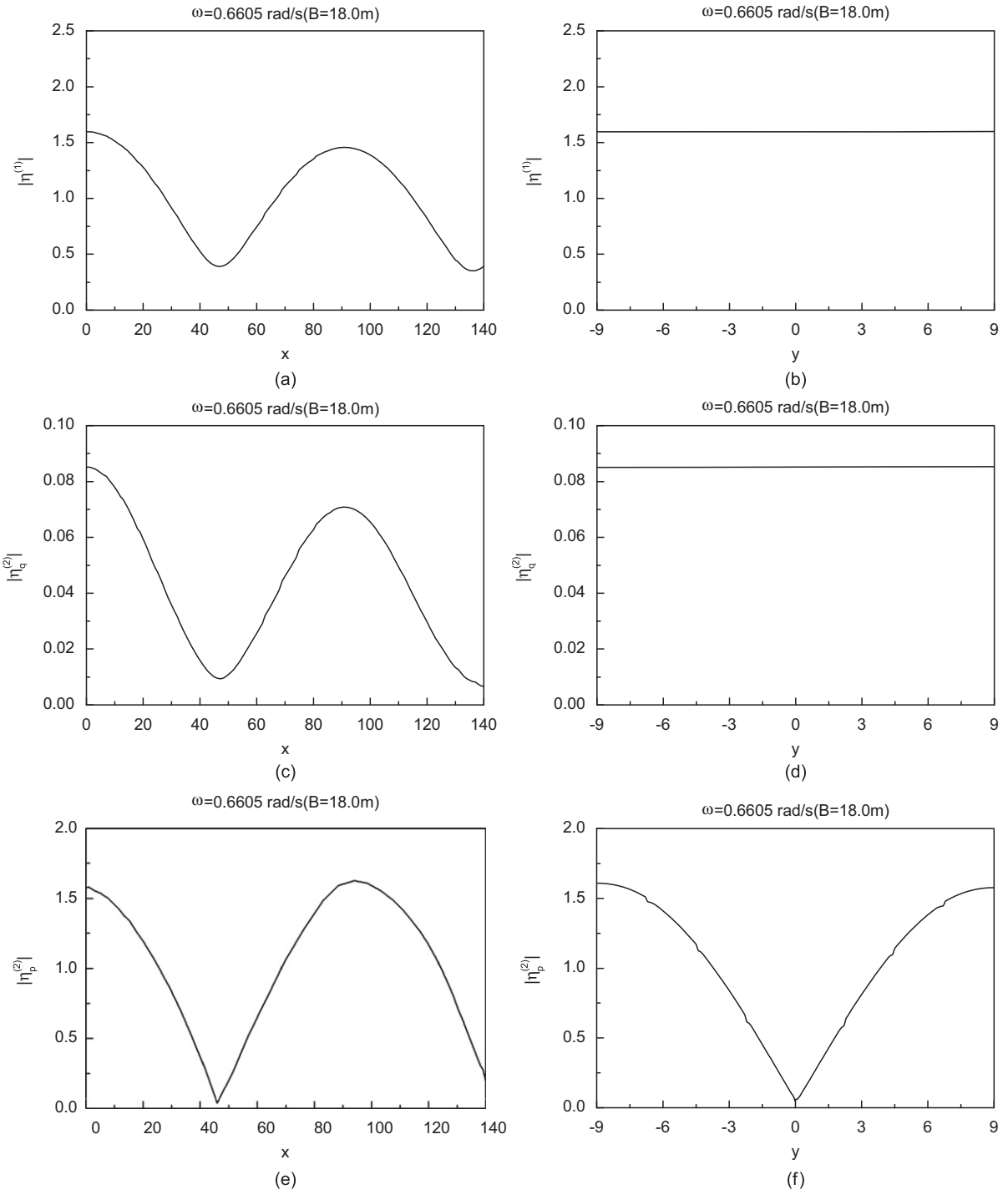

Fig. 27. Wave elevation in the gap between the two boxes. (a) first-order, (c) second-order quadratic, (e) second-order potential term along box 2 ($y = 9.0$ m), (b) first-order, (d) second-order quadratic and (f) second-order potential term across the gap ($x = 0$).

propagating wave along the gap becomes more significant, and this causes a slight shift in the peaks of the RAOs. With increase in draft of the two vessels, it was found that the frequencies of the symmetric gap mode peaks reduced substantially; however the location of the higher frequency antisymmetric mode peaks hardly changed at all.

The analytical work was focused on two extremely simple cases. The open-ended moonpool model provided very good predictions of the peak frequencies calculated with the full 3-D diffraction analysis at various drafts. The other simple case, based on theory for a channel in an infinite breakwater, provided not only resonant frequencies but also amplitudes. The resulting RAOs were remarkably close to those predicted by DIFFRACT for the two-box configuration.

Finally a study was made of second-order forces and elevations in the gap for the two-box problem. For very closely spaced boxes it was found that particularly careful attention must be paid to the associated calculation of a free-surface integral, but with appropriate meshes convergence was obtained. The results are consistent with the first-order behaviour: peaks in RAOs are formed at the discrete wave frequencies identified in the linear analysis, but also at half those frequencies because of the contribution from the second-order potential. It can be observed that, for the 18 m spacing case, the frequencies that are half those of the first few antisymmetric gap mode resonances lie close to the frequencies of low-order symmetric modes. It can be envisaged that, for a slightly different spacing, a second-order effect exciting an antisymmetric mode could occur at exactly the same frequency as a linear effect exciting a symmetric mode.

Overall the numerical results suggest that it is important not to ignore the resonant effects discussed here. While the amplifications in reality may be less than predicted using ideal flow theory, they can nevertheless be very significant. It should also be noted that any viscous damping effects that limit the free-surface resonant peaks predicted by the theory may not be as large at full scale as in model tests (although this speculation is as yet untested).

Acknowledgements

This work was supported by the SAFE OFFLOAD Project under EU Framework 6. The collaborative partners are Shell International Exploration and Production B.V., Instituto Superior Tecnico Lisbon, DHI, Det Norske Veritas A/S, Imperial College London, Lisnave Estaleiros Navais SA, Noble Denton Consultants Ltd., Ocean Wave Engineering Ltd., and Oxford University. The EU project is linked to a JIP supported by ABS, Bluewater, Daewoo, Petrobras, SBM and StatoilHydro.

References

Eatock Taylor, R., 2007. Hydroelastic analysis of plates and some approximations. Journal of Engineering Mathematics 58, 267–278.

Eatock Taylor, R., Chau, F.P., 1992. Wave diffraction theory—some developments in linear and non-linear theory. Journal of Offshore Mechanics and Arctic Engineering 114, 185–194.

Eatock Taylor, R., Huang, J.B., 1996. Practical computation of non-linear wave diffraction effects in offshore structures. In: Proceedings of the International Symposium on Offshore Engineering, Bandung, Indonesia.

Hong, S.Y., Kim, J.H., Cho, S.K., Choi, Y.R., Kim, Y.S., 2005. Numerical and experimental study on hydrodynamic interaction of side-by-side moored multiple vessels. Ocean Engineering 32, 783–801.

Howe, M.S., 2007. Hydrodynamics and Sound. Cambridge University Press, Cambridge.

Kashiwagi, M., 2007. 3-D calculation for multiple floating bodies in proximity using wave interaction theory. In: Proceedings of the 17th International Conference on Offshore and Polar Engineering, Lisbon, Portugal.

Kashiwagi, M., Endo, K., Yamaguchi, H., 2005. Wave drift forces and moments on two ships arranged side-by-side in waves. Ocean Engineering 32, 529–555.

Koo, B.J., Kim, M.H., 2005. Hydrodynamic interactions and relative motions of two floating platforms with mooring lines in side-by-side offloading operation. Applied Ocean Research 27, 292–310.

Kristiansen, T., Faltinsen, O.M., 2008. Application of a vortex tracking method to the piston-like behaviour in a semi-entrained vertical gap. Applied Ocean Research 30, 1–16.

Kristiansen, T., Faltinsen, O.M., 2007. Resonant water motion between a ship and a terminal in shallow water. In: Proceedings of the 26th International Conference on Offshore Mechanics and Arctic Engineering, San Diego, USA.

Lee, C.-H., Newman, J.N., 2005. Computation of wave effects using the panel method. In: Chakrabarti, S.K. (Ed.), Numerical Models in Fluid–Structure Interaction. WIT Press, Southampton, pp. 211–251.

Lu, L., Cheng, L., Teng, B., Li, Y., 2008. Numerical simulation of hydrodynamics resonance in narrow gap between twin bodies subject to water waves. In: Proceedings of the 18th International Offshore and Polar Engineering Conference Vancouver, Canada.

Mei, C.C., 1983. The Applied Dynamics of Ocean Surface Waves. World Scientific, Singapore.

Miao, G.-P., Saitoh, T., Ishida, H., 2001. Water wave interactions of twin large scale caissons with a small gap between. Coastal Engineering Journal 43, 39–58.

Molin, B., 2001. On the piston and sloshing modes of moonpools. Journal of Fluid Mechanics 430, 27–50.

Molin, B., Remy, F., Kimmoun, O., Stassen, Y., 2002. Experimental study of the wave propagation and decay in a channel through a rigid ice sheet. Applied Ocean Research 24, 247–260.

Newman, J.N., Sclavounos, P.D., 1988. The computation of wave loads on large offshore structures. In: Proceedings of the International Conference on Behaviour of Offshore Structures, BOSS88, vol. 2, pp. 605–619.

Pauw, W.H., Huijsmans, R.H.M., Voogt, A., 2007. Advances in the hydrodynamics of side-by-side moored vessels. In: Proceedings of the 26th International Conference on Offshore Mechanics and Arctic Engineering, San Diego, USA.

Saitoh, T., Ishida, H., Miao, G.-P., 2000. Influence of gaps between multiple floating bodies on wave forces. China Ocean Engineering 14, 407–422.

Saitoh, T., Miao, G.-P., Ishida, H., 2006. Resonance of fluid in narrow joint gaps of caisson-type seawall. In: Proceedings of the International Conference on Coastal Engineering, San Diego, USA.

Subia, S.R., Ingber, M.S., Mitra, A.K., 1995. A comparison of the semi-discontinuous element and multiple node with auxiliary boundary collocation approaches for the boundary element method. Engineering Analysis with Boundary Elements 15, 19–27.

Sulisz, W., Hudspeth, R.T., 1993. Complete second-order solution for water waves generated in wave flumes. Journal of Fluids and Structures 7, 253–268.

Sun, L., Teng, B., Liu, C.F., 2008a. Removing irregular frequencies by a partial discontinuous higher order boundary element method. Ocean Engineering 35, 920–930.

Sun, L., Taylor, P.H., Eatock Taylor, R., 2008b. First and second order wave effects in narrow gaps between moored vessels. In: Proceedings of the Marine Operations Specialty Symposium, MOSS2008, Singapore.

Teigen, P., Niedzwecki, J.M., 2006. A computational study of wave effects related to side-by-side LNG offloading. In: Proceedings of the 16th International Offshore and Polar Engineering Conference, San Francisco, USA.

Tromans, P.S., 2008. Roll damping of turret-moored vessels. Report D-5.2a(0)-OWE, EU Safe Offload Project.

Wang, C.Z., Wu, G.X., 2008. Analysis of second-order resonance in wave interactions with floating bodies through a finite-element method. Ocean Engineering 35, 717–726.

Zang, J., Gibson, R., Taylor, P.H., Eatock Taylor, R., Swan, C., 2006. Second order wave diffraction around a fixed ship-shaped body in unidirectional steep waves. Journal of Offshore Mechanics and Arctic Engineering 128, 89–99.

Zhang, S., Williams, A.N., 1996. Time-domain simulation of the generation and propagation of second-order Stokes waves in a two-dimensional wave flume. Part I: monochromatic wavemaker motions. Journal of Fluids and Structures 10, 319–335.

Zhu, R.-C., Miao, G.-P., You, Y.-X., 2005. Influence of gaps between 3-D multiple structures on wave forces. Journal of Hydrodynamics Series B 172, 141–147.

Zhu, R.-C., Miao, G.-P., Zhu, H.-R., 2006. The radiation problem of multiple structures with small gaps in between. Journal of Hydrodynamics Series B 185, 520–526.